

Photon-induced two-nucleon knockout reactions to discrete final states

C. Giusti and F.D. Pacati

*Dipartimento di Fisica Nucleare e Teorica, Università di Pavia, and
Istituto Nazionale di Fisica Nucleare, Sezione di Pavia, Pavia, Italy*

Abstract

Cross sections and photon asymmetries of the exclusive $^{16}\text{O}(\gamma, \text{pn})^{14}\text{N}$ and $^{16}\text{O}(\gamma, \text{pp})^{14}\text{C}$ knockout reactions are calculated for transitions to the low-lying discrete final states of the residual nucleus in the photon-energy range between 100 and 400 MeV. Exclusive reactions may represent a test of reaction mechanisms and a promising tool for investigating the dynamics of nucleon pairs in different states. Cross sections and asymmetries for both (γ, pn) and (γ, pp) turn out to be only slightly affected by short-range correlations and dominated by two-body currents. Therefore, two-nucleon knockout reactions induced by real photons appear well suited to investigate the nuclear current and the selectivity of individual transitions to its different components.

PACS numbers: 25.20.Lj, 24.50+g

1. INTRODUCTION

Electromagnetically induced two-nucleon knockout reactions have long been considered an important tool for investigating the properties of nucleon pairs within nuclei and their interaction at short distance [1,2].

Direct information on dynamical short-range correlations (SRC), which are linked to the short-ranged repulsive core of the NN-interaction, can be obtained if one assumes that the real or virtual photon hits, through a one-body current, either nucleon of a correlated pair and both nucleons are then ejected. However, nucleon pairs can also be ejected by two-nucleon currents, which effectively take into account the influence of subnuclear degrees of freedom like mesons and isobars. A reliable treatment of both these competing processes as well as of other reaction mechanisms is in principle needed before one can draw definite conclusions in comparison with data. However, since the role and relevance of these contributions is different in different reactions and kinematics, it is possible to envisage appropriate situations where various specific effects can be disentangled and separately investigated.

The most promising tool for studying SRC is represented by the $(e, e' \text{pp})$ reaction, where the effect of two-body currents is less dominant as compared to the $(e, e' \text{pn})$ and (γ, NN) processes. The first exploratory triple coincidence measurements of the $(e, e' \text{pp})$ cross section,

performed at NIKHEF on ^{12}C [3,4], gave clear evidence of two-nucleon knockout in the dip region. Peaks corresponding to knockout of protons from the $1p$ and $1s$ shells were clearly recognized in the missing-energy spectrum. The measured cross sections were found in satisfactory agreement with the model calculations of refs. [5,6] in the region corresponding to $(1p)^2$ knockout and indicated that a large part of the strength can be attributed to SRC. In most recent experiments on ^{16}O at NIKHEF [7,8] and Mainz [9] it was possible to achieve sufficient energy resolution to allow the separation of the cross section related to distinct states of ^{14}C . A further experiment on ^{16}O with improved statistics has been approved in Mainz [10]. The presence of discrete final states with well-defined angular momentum makes ^{16}O a particularly attractive target, since specific final states may act as filter for the study of different reaction processes involving SRC and two-nucleon currents [11,12]. Moreover, the first and so far only available calculation of the two-nucleon spectral function for a finite nucleus, has been applied just to ^{16}O [13]. The corresponding pair removal amplitudes have been included in the description of the $(\text{e},\text{e}'\text{pp})$ knockout reaction [12]. The predicted selectivity of the considered reaction involving different final states, which is confirmed by the fair agreement obtained in the first comparisons with data [8,9], opens up good perspectives for the study of SRC in $(\text{e},\text{e}'\text{pp})$ reactions.

The (γ,NN) reactions appear dominated by medium-range meson-exchange currents and a good understanding of the dominant single-pion-exchange mechanisms is essential before one can hope of investigating shorter range effects [14,15].

First exploratory (γ,NN) experiments performed in Bonn [16] and Tokio [17] had neither good statistical accuracy nor sufficient energy resolution to allow a straightforward investigation of direct processes. Early work in Mainz [18] had good energy resolution allowing the identification of nucleons emitted from different shells. Further experiments with good statistics and resolution were carried out in Mainz [19,20] and Lund [21] in order to disentangle the reaction mechanisms. A major conclusion was obtained through comparison of missing-energy spectra with the results of the theoretical model of ref. [22], where different contributing mechanisms are included in the description of the pion and nucleon photoproduction channels in a unified diagrammatic approach: only the low missing-energy region ($E_{2m} \leq 40$ MeV) is predominantly fed by direct photoabsorption on a nucleon pair, whereas for $E_{2m} \geq 70$ MeV other mechanisms, e.g. contributions originating from quasifree (γ,π) production and subsequent pion final-state interactions, become dominant. This result implies that only low values of E_{2m} must be considered when studying the properties of nucleon pairs and was qualitatively confirmed by the analysis of the data in ref. [20] through the model of ref. [14].

Measurements with sufficient energy resolution to separate the low-lying final states of the residual nucleus are of great interest also in the case of photon-induced reactions. They represent a stringent test of reaction models and allow one to investigate the state dependence of the photoabsorption process on nucleon pairs. However, most of the data collected up till now could not separate individual final states and simultaneously provide dependences of the cross sections on dynamical variables. The high-resolution experiments performed in Lund [21] for the $^{16}\text{O}(\gamma, \text{pn})^{14}\text{N}$ reaction could separate final states, but, owing to low statistics, no momentum distribution for even the strongest states could be obtained. A new high resolution experiment for the $^{16}\text{O}(\gamma, \text{pn})^{14}\text{N}$ and $^{16}\text{O}(\gamma, \text{pp})^{14}\text{C}$ reactions in the photon-energy range between 90 and 270 MeV, aiming at separating final states and at

determining also the momentum distributions for each state, has been recently approved in Mainz [23].

Various theoretical models have been developed over the last years to deal with two-nucleon emission processes. The model of ref. [22] aims at the best microscopic description of the photoabsorption process and includes many different reaction mechanisms. This approach is extremely useful to understand and disentangle the main mechanisms contributing in different kinematical regions and is able to reproduce their general features. However, it cannot describe the details of the nuclear structure aspects of the reaction, which are dealt with in a nuclear-matter approach with a local-density approximation. A detailed description of these aspects is essential if one wants to investigate the conditions of pairs of nucleons in finite nuclei and their state dependence through exclusive knockout reactions. A more proper description of nuclear structure properties is given by the two models developed in refs. [5,6] and [14,15], where, on the other hand, only the direct two-nucleon knockout mechanism is considered. Both of them include SRC, one-body and two-body currents and final-state interactions in a completely unfactorized calculation. These different aspects have been investigated at various steps and with somewhat different theoretical ingredients in the two models, which have both been applied to the analysis of existing data for electron- and photon-induced reactions.

In refs. [14,15] reactions to discrete final states are not explicitly investigated but in very particular situations. In refs. [5,6] the various approximations used in the calculations make it difficult to evaluate the cross sections for transitions to individual final states. Thus a sum over all contributions given by different pairs of nucleons in the same shell is performed, which experimentally corresponds to detect all the pairs of nucleons coming out of the considered shell. This assumption is largely compatible with the energy resolution of the first experiments, but is not adequate for the analysis of the most recent exclusive data already available for the $(e,e'pp)$ reaction [7-9] and of the new data that are becoming available for both electron- and photon-induced reactions [10,23].

Exclusive $(e,e'pp)$ reactions have been investigated in refs. [11,12]. In ref. [11] the theoretical model of refs. [5] has been improved with a full treatment of antisymmetrization and of spin and isospin couplings. In ref. [12] the pair removal amplitudes obtained from the calculation of the two-proton spectral function of ^{16}O [13] have been included in the reaction calculation. The treatment of the Δ isobar current is more specifically discussed in ref. [24], where some first numerical results for the exclusive (γ,pp) reaction are given but the spectral function is not included in the model.

In this paper results for the exclusive $^{16}\text{O}(\gamma, pn)^{14}\text{N}$ and $^{16}\text{O}(\gamma, pp)^{14}\text{C}$ reactions to individual low-lying discrete final states of the residual nucleus are presented and discussed. These two reactions appear of particular interest. Exclusive data for both of them are expected from an approved experiment in Mainz [23].

The approach already applied to the $^{16}\text{O}(e, e'pp)^{14}\text{C}$ reaction [12] is here applied to the $^{16}\text{O}(\gamma, pp)^{14}\text{C}$ reaction. In this approach the pair removal amplitudes are obtained from the calculation of the spectral function, where both long-range and short-range correlations are treated consistently. Different relative and center-of-mass (CM) states of the pair contribute to a specific transition. They can be separated in the calculation and their effects can individually be investigated. A calculation of the spectral function for a pn pair is not available yet. Thus for the $^{16}\text{O}(\gamma, pn)^{14}\text{N}$ reaction the simpler prescription of ref. [11] is

adopted here, where the two-nucleon overlap is given by the product of a coupled and fully antisymmetrized pair function of the shell model (SM) and a Jastrow type correlation function. In the two-body current for a pn pair contributions given by both seagull and pion-in-flight diagrams have been added to the Δ isobar current. This represents a further improvement with respect to the previous calculations for (γ, pn) reactions of ref. [6], where pion-in-flight diagrams were neglected. With respect to ref. [15], which is mainly devoted to investigate the quasi-deuteron kinematics and the behaviour of nucleon pairs knocked-out from different shells, this paper aims at investigating the transitions to discrete states, in order to explore their selectivity to the different components of the nuclear current. Moreover, the comparison of the results obtained with different models can give a deeper insight into the mechanisms of two-nucleon emission and the nuclear structure properties.

In this paper numerical results of cross sections and asymmetries are presented in the photon-energy range between 100 and 400 MeV. It was already observed in ref. [6] how the asymmetry of the cross section, that can be measured with linearly polarized photons, is helpful to investigate the reaction mechanism and the role of the different terms of the nuclear current. First asymmetry measurements for the $^{16}\text{O}(\gamma, \text{pp})$ and $^{16}\text{O}(\gamma, \text{pn})$ reactions have been carried out at LEGS [25] in the photon energy range between 245 and 315 MeV. At these energies, around the peak of Δ resonance, the contribution of the isobar current is dominant and the calculations are extremely sensitive to its treatment. The data indicate the need of a careful description of this important theoretical ingredient. In this first experiment, however, the energy resolution was not sufficient to separate final nuclear states.

The more refined treatment of spin degrees of freedom in the present approach is expected to give important effects on a polarization observable such as the asymmetry. It seems moreover interesting to investigate the dependence of this observable on the different states of the nucleon pair.

The theoretical approach is outlined in sect. 2. Numerical results for the $^{16}\text{O}(\gamma, \text{pn})^{14}\text{N}$ and $^{16}\text{O}(\gamma, \text{pp})^{14}\text{C}$ reactions are presented and discussed in sect. 3 and sect. 4, respectively. Some conclusions are drawn in sect. 5.

2. THEORETICAL APPROACH

The coincidence cross section for the reaction induced by a photon, with energy E_γ , where two nucleons, with momenta \mathbf{p}'_1 , and \mathbf{p}'_2 and energies E'_1 and E'_2 , are ejected from a nucleus, is given, after integrating over E'_2 , by [6,2]

$$\frac{d^5\sigma}{dE'_1 d\Omega'_1 d\Omega'_2} = \frac{\pi e^2}{2E_\gamma} \Omega_f f_{\text{rec}}^{-1} W_T, \quad (1)$$

where $\Omega_f = p'_1 E'_1 p'_2 E'_2$ is the phase-space factor and integration over E'_2 produces the recoil factor

$$f_{\text{rec}}^{-1} = 1 - \frac{E'_2}{E_B} \frac{\mathbf{p}'_2 \cdot \mathbf{p}_B}{|\mathbf{p}'_2|^2}, \quad (2)$$

where E_B and \mathbf{p}_B are the energy and momentum of the residual nucleus. The transverse structure function W_T , which only depends on E_γ , p'_1 , p'_2 , the angles γ_1 , between the momentum of the incident photon \mathbf{q} and \mathbf{p}'_1 , γ_2 , between \mathbf{q} and \mathbf{p}'_2 , and γ_{12} , between \mathbf{p}'_1 and \mathbf{p}'_2 , is expressed in terms of the components of the hadron tensor $W^{\mu\nu}$ [2], i.e.

$$W_T = W^{xx} + W^{yy} \quad (3)$$

and is thus given by bilinear combinations of the Fourier transforms of the transition matrix elements of the nuclear current density operator taken between initial and final nuclear states.

If the residual nucleus is left in a discrete eigenstate of its Hamiltonian, i.e. for an exclusive process, and under the assumption of a direct knockout mechanism, the transition matrix elements can be written as [5,11]

$$\begin{aligned} \mathbf{J}(\mathbf{q}) = & \int \psi_f^*(\mathbf{r}_1\sigma_1, \mathbf{r}_2\sigma_2) \mathbf{J}(\mathbf{r}, \mathbf{r}_1\sigma_1, \mathbf{r}_2\sigma_2) \psi_i(\mathbf{r}_1\sigma_1, \mathbf{r}_2\sigma_2) \\ & \times e^{i\mathbf{q}\cdot\mathbf{r}} d\mathbf{r} d\mathbf{r}_1 d\mathbf{r}_2 d\sigma_1 d\sigma_2. \end{aligned} \quad (4)$$

Eq. (4) contains three main ingredients: the two-nucleon overlap integral ψ_i , the nuclear current \mathbf{J} and the final-state wave function ψ_f .

The derivation of Eq. (4) involves bound and scattering states, ψ_i and ψ_f , which are consistently derived from an energy-dependent non-hermitian Feshbach-type Hamiltonian for the considered final state of the residual nucleus. They are eigenfunctions of this Hamiltonian at negative and positive energy eigenvalues, respectively [5,2]. In practice, it is not possible to achieve this consistency and the treatment of initial and final state correlations proceeds separately with different approximations.

In the final-state wave function ψ_f each of the outgoing nucleons interacts with the residual nucleus while the mutual interaction between the two outgoing nucleons is neglected. The scattering state is thus written as the product of two uncoupled single-particle distorted wave functions, eigenfunctions of a complex phenomenological optical potential which contains a central, a Coulomb and a spin-orbit term.

The two-nucleon overlap integral ψ_i contains the information on nuclear structure and allows one to write the cross section in terms of the two-hole spectral function [2]. Since only a calculation of the two-proton spectral function of ^{16}O is available at present [13,12], two different prescriptions have been here adopted for pp and pn knockout.

For the $^{16}\text{O}(\gamma, \text{pp})^{14}\text{C}$ reaction the two-nucleon overlap integrals are taken from the calculation of the spectral function [13,12]. They have been obtained from a two-step procedure, where long-range and short-range correlations are treated in a separate but consistent way. The calculation of long-range correlations is performed in a SM space large enough to incorporate the corresponding collective features which influence the pair removal amplitudes. The single-particle propagators used for this dressed Random Phase Approximation description of the two-particle propagator also include the effect of both long-range and short-range correlations. In the second step that part of the pair removal amplitudes which describes the relative motion of the pair is supplemented by defect functions obtained from the same G-matrix which is also used as the effective interaction in the RPA calculation.

For a discrete final state of the ^{14}C nucleus, with angular momentum quantum numbers JM , the two-nucleon overlap integral is expressed in terms of relative and CM wave functions as

$$\psi_i(\mathbf{r}_1\boldsymbol{\sigma}_1, \mathbf{r}_2\boldsymbol{\sigma}_2) = \sum_{nlSjNL} c_{nlSjNL}^i \phi_{nlSj}(r_{12}) R_{NL}(R) \left[\mathfrak{S}_{lS}^j(\Omega_r, \boldsymbol{\sigma}_1, \boldsymbol{\sigma}_2) Y_L(\Omega_R) \right]^{JM}, \quad (5)$$

where

$$\mathbf{r}_{12} = \mathbf{r}_1 - \mathbf{r}_2, \quad \mathbf{R} = \frac{(\mathbf{r}_1 + \mathbf{r}_2)}{2} \quad (6)$$

are the relative and CM variables. The brackets in Eq. (5) indicate angular momentum coupling of the angular and spin wave function \mathfrak{S} of relative motion with the spherical harmonic of the CM coordinate to the total angular momentum quantum numbers JM . The CM radial wave function R_{NL} is that of a harmonic oscillator (h.o.), with oscillator parameter $b = 1.77$ fm. SRC are included in the radial wave function ϕ of relative motion through a defect function defined by the difference between ϕ and the uncorrelated relative h.o. wave function of the pair R_{nl} , i.e. [13]

$$\phi_{nlSj}(r_{12}) = R_{nl}(r_{12}) + D_{lSj}(r_{12}). \quad (7)$$

These defect wave functions were obtained by solving the Bethe-Goldstone equation in momentum space for ^{16}O [26]. They depend on different quantum numbers l, S, l . In the following the partial wave notation $^{2S+1}l_j$, for $l = S, P, D$, is used for the relative states.

The coefficients c^i in Eq. (5) contain contributions from a SM space which includes the $0s$ up to the $1p0f$ shells. More details are given in ref. [13] and in ref. [12], where the same approach is applied to the reaction $^{16}\text{O}(\text{e}, \text{e}'\text{pp})^{14}\text{C}$.

For the reaction $^{16}\text{O}(\gamma, \text{pn})^{14}\text{N}$, where a calculation of the spectral function is not available, the simpler prescription already applied in ref. [11] to $(\text{e}, \text{e}'\text{pp})$ has been adopted here. The two-nucleon overlap is thus given by

$$\psi_i(\mathbf{r}_1\boldsymbol{\sigma}_1, \mathbf{r}_2\boldsymbol{\sigma}_2) \simeq \Phi_{JM}(\mathbf{r}_1\boldsymbol{\sigma}_1, \mathbf{r}_2\boldsymbol{\sigma}_2) f(r_{12}) X_{TT_3}(\tau_1, \tau_2), \quad (8)$$

where $\Phi_{JM} X_{TT_3}$ is the coupled and fully antisymmetrized pair function of the shell model, X_{TT_3} is its isospin part and f is a correlation function of Jastrow type which incorporates SRC. Only the central part of the correlation function is retained in the calculations. Thus long-range correlations are not included in this simpler approach. The overlap function of Eq. (8) describes a pair of nucleons ejected from the same or different shells. The model includes the spectral strength λ . In the calculations we have assumed $\lambda = 1$.

The nuclear current operator in Eq. (4) is the sum of a one-body and a two-body part. In the one-body part convective and spin currents are included. The two-body current is derived from the effective Lagrangian of ref. [27], performing a non relativistic reduction of the lowest-order Feynman diagrams with one-pion exchange. We have thus currents corresponding to the seagull and pion-in-flight diagrams and to the diagrams with intermediate isobar configurations, i.e.

$$\begin{aligned} \mathbf{J}^{(2)}(\mathbf{r}, \mathbf{r}_1\boldsymbol{\sigma}_1, \mathbf{r}_2\boldsymbol{\sigma}_2) = & \mathbf{J}^{\text{sea}}(\mathbf{r}, \mathbf{r}_1\boldsymbol{\sigma}_1, \mathbf{r}_2\boldsymbol{\sigma}_2) + \mathbf{J}^{\pi}(\mathbf{r}, \mathbf{r}_1\boldsymbol{\sigma}_1, \mathbf{r}_2\boldsymbol{\sigma}_2) \\ & + \mathbf{J}^{\Delta}(\mathbf{r}, \mathbf{r}_1\boldsymbol{\sigma}_1, \mathbf{r}_2\boldsymbol{\sigma}_2). \end{aligned} \quad (9)$$

In the coordinate space the seagull and pion-in-flight currents are [2]

$$\begin{aligned} \mathbf{J}^{\text{sea}}(\mathbf{r}, \mathbf{r}_1 \boldsymbol{\sigma}_1, \mathbf{r}_2 \boldsymbol{\sigma}_2) &= -\frac{f^2}{4\pi} (\boldsymbol{\tau}_1 \times \boldsymbol{\tau}_2)_3 [\boldsymbol{\sigma}^{(1)} \delta(\mathbf{r}_1 - \mathbf{r}) (\boldsymbol{\sigma}^{(2)} \cdot \hat{\mathbf{r}}_{12})] \\ &\times \left(1 + \frac{1}{\mu r_{12}}\right) \frac{e^{-\mu r_{12}}}{\mu r_{12}} + (1 \leftrightarrow 2), \end{aligned} \quad (10)$$

$$\begin{aligned} \mathbf{J}^\pi(\mathbf{r}, \mathbf{r}_1 \boldsymbol{\sigma}_1, \mathbf{r}_2 \boldsymbol{\sigma}_2) &= -\frac{f^2}{16\pi^2} (\boldsymbol{\tau}_1 \times \boldsymbol{\tau}_2)_3 \nabla_1 (\boldsymbol{\sigma}_1 \cdot \nabla_1) (\boldsymbol{\sigma}_2 \cdot \nabla_2) \\ &\times \frac{e^{-\mu|\mathbf{r}_1 - \mathbf{r}|}}{\mu|\mathbf{r}_1 - \mathbf{r}|} \frac{e^{-\mu|\mathbf{r}_2 - \mathbf{r}|}}{\mu|\mathbf{r}_2 - \mathbf{r}|} + (1 \leftrightarrow 2), \end{aligned} \quad (11)$$

where $f^2/(4\pi) = 0.079$ and μ is the pion mass.

The operator form of the Δ current has been derived in ref. [24]. It is given by the sum of the contributions of two types of processes, corresponding to the Δ -excitation and Δ -deexcitation currents. The first process (I) describes Δ -excitation by photon absorption and subsequent deexcitation by pion exchange, while the second (II) describes the time interchange of the two steps, i.e., first excitation of a virtual Δ by pion exchange in a NN collision and subsequent deexcitation by photon absorption. The propagator of the resonance, G_Δ , depends on the invariant energy \sqrt{s} of the Δ , which is different for processes I and II. For the deexcitation current the static approximation can be applied, i.e.

$$G_\Delta^{\text{II}} = (M_\Delta - M)^{-1}, \quad (12)$$

where $M_\Delta = 1232$ MeV. For the excitation current we use [28]

$$G_\Delta^{\text{I}} = \left(M_\Delta - \sqrt{s_{\text{I}}} - \frac{i}{2} \Gamma_\Delta(\sqrt{s_{\text{I}}}) \right)^{-1}, \quad (13)$$

with

$$\sqrt{s_{\text{I}}} = \sqrt{s_{\text{NN}}} - M, \quad (14)$$

where $\sqrt{s_{\text{NN}}}$ is the experimentally measured invariant energy of the two outgoing nucleons and the energy-dependent decay width of the Δ , Γ_Δ , has been taken in the calculations according to the parameterization of ref. [29].

The sum of the two processes gives

$$\begin{aligned} \mathbf{J}^\Delta(\mathbf{r}, \mathbf{r}_1 \boldsymbol{\sigma}_1, \mathbf{r}_2 \boldsymbol{\sigma}_2) &= \gamma \delta(\mathbf{r} - \mathbf{r}_1) \{ i(G_\Delta^{\text{I}} + G_\Delta^{\text{II}}) [4\tau_{2,3} \mathbf{A}(\mathbf{r}_{12}, \boldsymbol{\sigma}_1, \boldsymbol{\sigma}_2) - (\boldsymbol{\tau}_1 \times \boldsymbol{\tau}_2)_3 \\ &\times \mathbf{B}(\mathbf{r}_{12}, \boldsymbol{\sigma}_1, \boldsymbol{\sigma}_2)] + 2(G_\Delta^{\text{I}} - G_\Delta^{\text{II}}) [(\boldsymbol{\tau}_1 \times \boldsymbol{\tau}_2)_3 \mathbf{A}(\mathbf{r}_{12}, \boldsymbol{\sigma}_1, \boldsymbol{\sigma}_2) \\ &+ \tau_{2,3} \mathbf{B}(\mathbf{r}_{12}, \boldsymbol{\sigma}_1, \boldsymbol{\sigma}_2)] \} + (1 \leftrightarrow 2), \end{aligned} \quad (15)$$

where

$$\mathbf{A}(\mathbf{r}_{12}, \boldsymbol{\sigma}_1, \boldsymbol{\sigma}_2) = (\mathbf{q} \times \hat{\mathbf{r}}_{12}) (\boldsymbol{\sigma}_2 \cdot \hat{\mathbf{r}}_{12}) Y^{(1)}(r_{12}) - (\mathbf{q} \times \boldsymbol{\sigma}_2) Y^{(2)}(r_{12}), \quad (16)$$

$$\mathbf{B}(\mathbf{r}_{12}, \boldsymbol{\sigma}_1, \boldsymbol{\sigma}_2) = \mathbf{q} \times (\boldsymbol{\sigma}_1 \times \hat{\mathbf{r}}_{12}) (\boldsymbol{\sigma}_2 \cdot \hat{\mathbf{r}}_{12}) Y^{(1)}(r_{12}) - \mathbf{q} \times (\boldsymbol{\sigma}_1 \times \boldsymbol{\sigma}_2) Y^{(2)}(r_{12}), \quad (17)$$

$$Y^{(1)}(r_{12}) = \left(1 + \frac{3}{\mu r_{12}} + \frac{3}{\mu^2 r_{12}^2}\right) \frac{e^{-\mu r_{12}}}{\mu r_{12}}, \quad (18)$$

$$Y^{(2)}(r_{12}) = \left(\frac{1}{\mu r_{12}} + \frac{1}{\mu^2 r_{12}^2}\right) \frac{e^{-\mu r_{12}}}{\mu r_{12}}, \quad (19)$$

and the factor γ collects various coupling constants

$$\gamma = \frac{f_{\gamma N\Delta} f_{\pi NN} f_{\pi N\Delta}}{36\pi\mu}. \quad (20)$$

The charge-exchange term $(\boldsymbol{\tau}_1 \times \boldsymbol{\tau}_2)_3$ in the two-body current vanishes for a pp pair. Thus only a part of the Δ current in Eq. (15) contributes to (γ, pp) reactions, whereas all the terms in eqs. (10,11,15) contribute to (γ, pn) . On this basis it is generally expected that the two-body current is much more important for the knockout of a pn pair than of a pp pair.

From the analysis of the isospin matrix structure of processes I and II, it can be understood [24] that for photon absorption on a pn pair only the excitation current contributes in a state with $T = 0$, whereas only the deexcitation current contributes in a state with $T = 1$. Since the propagator G_Δ^I gives rise to a pronounced resonant behaviour of the matrix elements of the excitation current in the photon-energy region between 200 and 400 MeV, we expect that in this region the contribution of the Δ current for the knockout of a pn pair with $T = 0$ is much larger than for a pn pair with $T = 1$.

Both processes I and II contribute to photon absorption on a pp pair ($T = 1$). For the knockout of a pp pair in a relative 1S_0 state the generally dominant magnetic dipole $NN \leftrightarrow N\Delta$ transition is suppressed because of total angular momentum and parity conservation [30]. In our calculations contributions of all multipoles are included through the term $e^{i\mathbf{q} \cdot \mathbf{r}}$, which represents the incident photon in the transition amplitudes of Eq. (4). Only if we set $e^{i\mathbf{q} \cdot \mathbf{r}} = 1$ the calculation for the Δ current is restricted to a magnetic-dipole transition. In any case the effect of higher multipoles is generally smaller and for a 1S_0 pp pair the Δ current, although nonvanishing, turns out to be much less important than for other relative states. This was already observed in ref. [12] for the $(e, e' \text{pp})$ reaction. In that case the contribution of the excitation current, which is generally dominant, is strongly reduced on a 1S_0 pp pair, where it becomes of about the same size or even smaller than that of the deexcitation current, which is generally small. As a consequence, in $(e, e' \text{pp})$ reactions situations where the removal of a 1S_0 pair is dominant are particularly well suited to emphasize and thus investigate effects of SRC [7,12]. This conclusion cannot be directly applied to (γ, pp) reactions, where only the transverse component of the nuclear response contributes and the longitudinal component, where the effects of SRC show up more strongly, is absent.

In photon-induced reactions with linearly polarized photons one can measure the photon asymmetry Σ , given by the difference between the cross sections with linear photon polarization parallel and perpendicular to the reaction plane. It can also be expressed in terms of the ratio between the two transverse structure functions W_{TT} and W_T [6,2], as

$$\Sigma = \frac{W^{xx} - W^{yy}}{W^{xx} + W^{yy}} = \frac{W_{TT}}{W_T}. \quad (21)$$

The asymmetry is particularly sensitive to spin variables and thus to the different terms of the nuclear current and to their interference, whose effects on W_T and W_{TT} are emphasized in the ratio, where, on the contrary, other effects are smoothed out [6,15].

In the following numerical results are presented of cross sections and asymmetries for the $^{16}\text{O}(\gamma, \text{pn})^{14}\text{N}$ and $^{16}\text{O}(\gamma, \text{pp})^{14}\text{C}$ reactions for transitions to discrete final states of the residual nucleus. High-resolution experiments are needed to separate individual final states in the excitation-energy spectrum. In our calculations each state is characterized by a particular value of the missing energy, given by

$$E_{2m} = E_\gamma - T'_1 - T'_2 - T_B = E_s + E_x, \quad (22)$$

where T'_1 , T'_2 and T_B are the kinetic energies of the two outgoing nucleons and of the residual nucleus, respectively, E_s is the separation energy at threshold for two-nucleon emission and E_x is the excitation energy of the residual nucleus.

3. THE REACTION $^{16}\text{O}(\gamma, \text{pn})^{14}\text{N}$

The theoretical approach for two-nucleon knockout outlined in sect. 2 has been applied to the reaction $^{16}\text{O}(\gamma, \text{pn})^{14}\text{N}$, for transitions to discrete final states of the residual nucleus. Only the states with an excitation energy lower than 12 MeV have been considered in the calculations, according to the experimental analysis of ref. [19], where the direct two-nucleon knockout mechanism is well established for missing energies up to 40 MeV in ^{12}C . Therefore we consider here transitions to the 1_1^+ ($T = 0$) ground state of ^{14}N , to the 0^+ ($T = 1$) state at 2.31 MeV, to the 1_2^+ ($T = 0$) state at 3.95 MeV, to the 2^+ ($T = 0$) state at 7.03 MeV and to the 3^+ ($T = 0$) state at 11.05 MeV. We do not consider the negative parity states at low energy and other positive parity states, as they are not assumed as two-hole states in the independent particle model and therefore are not likely to be excited in a direct knockout [31].

The two-nucleon overlap is taken in the calculations according to the prescription of Eq. (8). In the SM wave function, all the considered states are described as two-hole states in the p shell: 1_1^+ and 0^+ are $(p_{1/2})^{-2}$ holes, 1_2^+ and 2^+ are $(p_{1/2}p_{3/2})^{-1}$ holes and 3^+ is a $(p_{3/2})^{-2}$ hole. In the frame of a h.o. basis, their different components in the relative and CM motion are given in Table I with the corresponding amplitudes. This decomposition can be helpful to understand the general features of cross sections and asymmetries. In the calculations, however, the more realistic Woods-Saxon single-particle wave functions of ref. [33] have been used. The correlation function is taken from ref. [34].

The distorted wave functions in the final state are eigenfunctions of the optical potential of ref. [32], which includes also the spin-orbit component.

As explained in sect. 2, the nuclear current is the sum of a one-body part, whose contribution is entirely due to the correlation function, and a two-body part, including contributions of the lowest-order diagrams with one-pion exchange, i.e. seagull, pion-in-flight and diagrams with intermediate isobar configurations.

Calculations have been performed in the coplanar symmetrical kinematics, where the two nucleons are emitted in the scattering plane at equal energies and equal but opposite angles with respect to the beam direction, i.e. with $\gamma_1 = \gamma_2$ and $\gamma_{12} = \gamma_1 + \gamma_2$. In this kinematics, if E_γ is fixed and γ_1 is varied, it is possible to explore, for different scattering angles, all possible values of the recoil (p_B) or missing momentum (p_{2m}) distribution, where

$$\mathbf{p}_{2m} = \mathbf{p}_B = \mathbf{q} - \mathbf{p}'_1 - \mathbf{p}'_2. \quad (23)$$

If relative and CM motion are factorized and final-state interactions are neglected [1], \mathbf{p}_B is opposite to the total momentum \mathbf{P} of the nucleon pair in the target.

The choice of this kinematics is made at variance with that of ref. [15], where particular attention is drawn to the dynamics of dinucleons in the medium, which is studied through a kinematics where \mathbf{p}_B equals zero. The symmetrical kinematics is best suited to give information on the motion of the pair in different CM and relative angular momentum states and therefore to evaluate the effects of the one-body and two-body components of the nuclear current on these states, which is a goal of this paper.

The calculated cross sections allow us to investigate a missing-momentum range up to about 250-300 MeV/c on both sides of the distributions. A wide range of photon energies, between 100 and 400 MeV, has been explored.

The angular distributions corresponding to the five considered final states are given at $E_\gamma=100$ MeV in Figs. 1 and 2 and at $E_\gamma=300$ MeV in Figs. 3 and 4. In the figures separate contributions of the different terms of the nuclear current are compared with the cross sections produced by the sum of all of them. Moreover also the sum of the seagull and pion-in-flight currents and their sum with the one-body current are drawn, in order to better evaluate interference effects. The dependence on the photon energy in the considered range is given in Figs. 5 and 6, for the different contributions, at a fixed value of γ_1 near to the maximum of the distribution of each state.

The shape of the angular distributions in Figs. 1-4 is determined by the combined effect of the CM wave function of the pair and of the different terms of the nuclear current. The main effect is given by the components of the CM wave function contributing to each state: 0^+ and 1_2^+ have essentially an s -wave shape, 1_1^+ is due to a combination of p , d and s waves, while 2^+ and 3^+ are a combination of d and s waves at $E_\gamma = 100$ MeV and have a d -wave shape at $E_\gamma = 300$ MeV, where the contribution of the Δ current is dominant. This analysis is consistent with the decomposition presented in Table I, for h.o. shell model wave functions, combined with the different values of the nuclear current matrix elements of the different relative states.

The results in Figs. 1-4 indicate that the contribution of the one-body current and thus of SRC on the cross section is generally extremely small. It increases with the photon energy but is always overwhelmed by the two-body current. It is very sensitive to the choice of the correlation function: the strong correlation function of ref. [35] calculated with the hard-core OMY NN-interaction [36], for instance, can enhance the contribution of the one-body current by about an order of magnitude. Even in this case, however, the calculated cross sections are dominated by two-body currents. The use in the present approach for pn knockout of a central and state-independent correlation function represents a very simple description of SRC. Moreover these correlation functions are not specifically calculated for a pn pair. Nevertheless, this simple treatment should be able to give a reasonable prediction of the role of SRC in the considered situations. Our numerical results indicate that (γ, pn) cross sections are dominated by two-body currents and a more sophisticated treatment of correlations should not change this conclusion. This result is in agreement with that of refs. [15,25].

The seagull current is dominant, for all the considered transitions, at $E_\gamma = 100$ MeV and in general at low values of the photon energy, up to about 150 MeV. Its pure contribution

slightly decreases when the photon energy increases. The contribution of the pion-in-flight current is always much smaller than that of the seagull current and is only weakly dependent on the photon energy. It was found in refs. [14,15] that a destructive interference is given by the sum of these two terms. This result is confirmed by the present calculations. However here this effect is generally small, but for the 0^+ state, i.e. the only state with $T = 1$, where a strong destructive interference is obtained.

The isobar current shows, as expected, a strong dependence on the photon energy. Its contribution is negligible at low values of E_γ , as in Figs. 1 and 2, but gains importance as the energy increases and becomes dominant above 200 MeV. For the four states with $T = 0$ only the Δ -excitation current with its resonant propagator contributes. The resonance peak is clearly shown in the energy distributions of Figs. 5-6. On the contrary, only the Δ -deexcitation current contributes for the 0^+ ($T = 1$) state. Indeed for this state the Δ current does not show a resonant behaviour and above the pion-production threshold its contribution, although still dominant in the photon-energy range between 250 and 400 MeV, is smaller than for the other states.

In Figs. 7-10 the photon asymmetries are shown in the same situations and in the same conditions as in Figs. 1-4 for the cross section. Different shapes are obtained for different states. The asymmetry is sensitive to the nuclear current, whose different effects on the two structure functions W_T and W_{TT} in Eq. (21) are emphasized in the ratio. The differences between the results in Figs. 7 and 8, at $E_\gamma = 100$ MeV, and in Figs. 9 and 10, at $E_\gamma = 300$ MeV, indicate the role of the different terms of the nuclear current at the two values of the photon energy.

The asymmetry given by the contribution of the various terms of the current does not show a strong dependence on the photon energy. Like the cross section, it is not significantly affected by the one-body current. On the contrary, as it was already observed in the different model of ref. [15], it is very sensitive to all the components of the two-body current and to their interference. The pure contributions of the seagull and pion-in-flight currents generally give a positive asymmetry. In particular, for the seagull current it is positive and large (close to 1) for the 0^+ state and positive and small (around 0) for the 2^+ state. A large effect is given by the interference between seagull and pion-in-flight terms, which generally produces a negative asymmetry. Only for the 0^+ state the asymmetry given by the sum of the two terms remains positive. This strong interference effect is essential to produce the final result at low values of E_γ , e.g. in Figs. 7 and 8 at $E_\gamma = 100$ Mev. The contribution of the pion-in-flight terms and of its interference with the seagull current is therefore much more important for the asymmetry than for the cross section. The asymmetry produced by the Δ current is generally negative for all the considered states. In the calculations, however, it presents anomalies and sharp peaks corresponding to minima of the cross section. At large values of the photon energy, e.g. in Figs. 9 and 10 at 300 MeV, the asymmetry, like the cross section, is dominated by the Δ current. However, for the 0^+ state, where only the deexcitation part of the isobar current contributes, the effect of the other terms of the two-body current is relatively a bit more important in determining the final result.

4. THE REACTION $^{16}\text{O}(\gamma, \text{pp})^{14}\text{C}$

For the reaction $^{16}\text{O}(\gamma, \text{pp})^{14}\text{C}$ the theoretical approach of sect. 2 has been applied to the transitions to the three lowest discrete final states of the residual nucleus, i.e. the 0^+ ground state of ^{14}C , the 2^+ state at 7.01 MeV and the 1^+ state at 11.31 MeV. These are the states that have already been experimentally separated in the $^{16}\text{O}(\text{e}, \text{e}'\text{pp})^{14}\text{C}$ reaction [7,8,9].

The two-nucleon overlap functions for each state are taken in the calculations from the spectral function of refs. [13,12]. Their explicit expressions, Eq. (5), allow the separation of the different components of relative and CM motion. In Table II the main components and their amplitudes are given and compared with the corresponding amplitudes obtained, with h.o. wave functions, in the SM, where the states are described as two holes in the p shell: 0^+ is a $(p_{1/2})^{-2}$ hole, while 2^+ and 1^+ are $(p_{1/2}p_{3/2})^{-1}$ holes. While the SM amplitudes are normalized to one, the spectral density amplitudes are normalized to the spectroscopic factor, i.e. to about 0.6. The table shows that in the spectral function the amplitudes for the 3P_j relative states are more reduced than for the 1S_0 states with respect to the corresponding SM amplitudes. Other components, not shown in the table, contribute to the spectral density function and are included in the calculation, but their contribution is less than 1% [13,12].

The same conditions and the same ingredients used for the (γ, pn) reaction in sect. 3 have been adopted. For a pp pair, however, the two-body part of the nuclear current does not include the charge-exchange terms and contains only the non-exchange component of the Δ isobar current.

In order to explore the missing-momentum distribution of each state, the same coplanar symmetrical kinematics as in sect. 3 has been considered, with the same range of photon energies and scattering angles.

The angular distributions corresponding to the considered final states of ^{14}C are given in Figs. 11 and 12, at $E_\gamma = 100$ MeV, and in Fig. 13, at $E_\gamma = 300$ MeV. In Fig. 11 the separate contributions of the one-body and Δ currents are compared with the cross sections given by the sum of the two terms. In Figs. 12 and 13 the contributions of the different relative states are drawn.

The shape of the angular distributions is determined by the CM orbital angular momentum of the knocked-out pair. The 0^+ state has essentially an s -wave shape; the p -wave component becomes more important at large values of the missing momentum, where the s -wave contribution becomes small. The 1^+ state has a p -wave shape and the 2^+ state is a combination of p and d waves.

The Δ current is dominant in the cross section, for all the considered transitions and photon-energy values. Its contribution strongly increases with the energy, and above the pion-production threshold shows a pronounced resonant behaviour, with a maximum at the peak of the resonance. It is reduced in the 1S_0 state, where, as explained in sect. 2, the magnetic dipole $NN \leftrightarrow N\Delta$ transition is forbidden.

The contribution of the one-body current and therefore the effect of SRC is generally very small. SRC are accounted for in the calculations by defect functions which depend on the relative states. The results of Figs. 11-13 have been obtained with the defect functions calculated with the Bonn-A potential [13]. A different choice sensibly changes the contribution of the one-body current, but does only slightly influence the final result, which is driven

by the Δ current. An example is shown in Fig. 14, where the cross sections obtained with the defect functions from Bonn-A and Reid Soft Core potentials [13] are compared, for the 0^+ and 2^+ states, at $E_\gamma = 100$ MeV where the contribution of the Δ current is smaller. At higher energies the one-body contribution increases and the results with Reid defect functions become larger than with Bonn-A. The increase with the energy of the contribution of the Δ current is however much larger and the final cross sections are even more dominated by the two-body current. Our results indicate that also (γ,pp) cross sections are only slightly sensitive to SRC in the considered situations.

In Fig. 15 the photon asymmetries are shown for the 1^+ and 2^+ states at $E_\gamma = 100$ and 300 MeV. The contributions of the different relative states are shown with the same convention as in Figs. 12 and 13. For the 0^+ state, not drawn in the figure, the asymmetry is always negative and almost everywhere equal to -1 . This result was already observed in ref. [15].

The asymmetry, like the cross section, is dominated by the Δ current and does not show a strong dependence on the photon energy. Different results are obtained for different states. For 2^+ the asymmetry is negative, while for 1^+ it is large and positive, in agreement with the results of ref. [15], due to the large positive value (about 1) produced by the Δ current in the 3P_0 state, which gives the dominant contribution to the final result.

The asymmetry is not significantly affected by the one-body current. In Fig. 16 the effect of the different choices of the defect functions from Bonn-A and Reid potentials is shown for the 2^+ state at $E_\gamma = 100$ MeV. It appears that the choice of the defect functions can have a significant but not substantial effect on the asymmetry, confirming that (γ,NN) reactions are not particularly well suited for studying SRC.

5. SUMMARY AND CONCLUSIONS

In this paper exclusive ${}^{16}\text{O}(\gamma, \text{pn}){}^{14}\text{N}$ and ${}^{16}\text{O}(\gamma, \text{pp}){}^{14}\text{C}$ knockout reactions have been investigated, for transitions to the low-lying discrete final states of the residual nucleus.

Exclusive (γ,NN) reactions may represent a stringent test of reaction mechanisms and a promising tool for investigating the dynamics of bound pairs of nucleons in the nuclear medium. The presence of several discrete final states with well-defined angular momentum makes the ${}^{16}\text{O}$ nucleus an excellent target for this analysis. Measurements with sufficient energy resolution to separate individual final states and good statistical accuracy to determine for each state the dependence of the cross sections on dynamical variables are needed. These data are now becoming available from new high-resolution experiments [23].

Numerical predictions of cross sections and photon asymmetries have been presented in the photon-energy range between 100 and 400 MeV. These results have been obtained in a direct knockout framework where both one-body and two-body currents are included. The contribution of the one-body current is entirely due to SRC; the two-body terms include contributions of the lowest-order Feynman diagrams with one-pion exchange, i.e. seagull, pion-in-flight and diagrams with intermediate isobar configurations, where a Δ is excited or a preformed Δ is deexcited after the absorption of the photon. Final-state interactions are taken into account by means of a phenomenological spin-dependent optical potential

describing the interaction of each of the outgoing nucleons with the residual nucleus. The two-nucleon overlap functions have been obtained for the $^{16}\text{O}(\gamma, \text{pp})^{14}\text{C}$ reaction from a recent calculation of the spectral function [13], where both long-range and short-range correlations are consistently treated. This approach was already applied to the $^{16}\text{O}(\text{e}, \text{e}'\text{pp})^{14}\text{C}$ reaction [12]. The two-nucleon overlap functions for the $^{16}\text{O}(\gamma, \text{pn})^{14}\text{N}$ reaction are given by the product of a coupled and fully antisymmetrized SM pair function and a Jastrow type correlation function, which incorporates SRC, since a calculation of the spectral function for a pn pair is not available. Although presumably too simplistic, this prescription should be able to give reasonable predictions of the role of SRC in (γ, pn) reactions.

The angular distributions of the cross sections for transitions to different states have different shapes, essentially determined by the components of the CM orbital angular momentum of the initial pair. Also the asymmetry is sensitive to the behaviour of the different components of the pair wave functions. These results confirm that exclusive reactions are particularly well suited to check the relevance of the direct knockout mechanism and to explore the conditions of different pairs of nucleons in the nuclear medium.

Cross sections and asymmetries, for both (γ, pn) and (γ, pp) reactions, are only slightly affected by SRC and are dominated, in all the considered situations, by two-body currents. Therefore photon-induced two-nucleon knockout reactions do not seem particularly well suited to investigate SRC, but might give interesting information on the various terms of the nuclear current and on their behaviour in different kinematic conditions and in different states.

Better information on correlations for a pn pair might be obtained from the $(\text{e}, \text{e}'\text{pn})$ reactions, where also the longitudinal component of the nuclear response contributes. In this case, as it was already observed in $(\text{e}, \text{e}'\text{pp})$ [12], a suitable choice of kinematics in exclusive experiments might allow the separation of effects due to SRC and two-body currents. For this analysis, however, a more refined treatment of correlations would be desirable, such as that applied here to pp pairs through the spectral function. Moreover, also tensor correlations might be investigated for nucleon pairs in a $T = 0$ state.

Our results indicate that in the $^{16}\text{O}(\gamma, \text{pn})^{14}\text{N}$ reaction the seagull current is dominant at lower values of the photon energy, up to about 150 MeV, then the Δ current gains importance. The contribution of the pion-in-flight current is always much smaller than that of the seagull current and is only weakly dependent on the photon energy. In the cross sections it generally produces a destructive interference with the seagull currents. This effect is however small, but for the 0^+ ($T = 1$) state. Interference effects are better emphasized in the photon asymmetry, where the interference between seagull and pion-in flight terms turns the asymmetry from positive, for both separate contributions, to negative, but for the 0^+ state. This effect is essential at low values of the photon energy, while at higher energies both cross sections and asymmetries are dominated by the Δ current. The Δ current is dominant also in the $^{16}\text{O}(\gamma, \text{pp})^{14}\text{C}$ reaction, for all the considered transitions and over all the considered range of photon energy. Its contribution strongly increases with the energy, but plays the main role, both on cross sections and asymmetries, even at 100 MeV.

The results of our investigation indicate that a good description of the isobar current is indispensable in the theoretical treatment. On the other hand, (γ, NN) reactions might give deeper insight into the behaviour of the Δ in the nuclear medium. Moreover, also the influence of two-body currents due to heavier meson exchange could deserve further investi-

tigation.

We are grateful to K. Allaart and P. Grabmayr for useful comments and fruitful discussions.

REFERENCES

- [1] K. Gottfried, Nucl. Phys. 5 (1958) 557; Ann. of Phys. 21 (1963) 29; W. Czyz and K. Gottfried Ann. of Phys. 21 (1963) 29; Y.N. Srivastava, Phys. Rev. 135 (1964) B612; D.U.L. Yu, Ann. of Phys. 38 (1966) 392.
- [2] S. Boffi, C. Giusti, F.D. Pacati and M. Radici, Electromagnetic response of atomic nuclei, Oxford Studies in Nuclear Physics (Clarendon Press, Oxford, 1996).
- [3] L.J.H.M. Kester, W.H.A. Hesselink, N. Kalantar-Nayestanaki, J.H. Mitchell, A. Pellegrino, E. Jans, J. Konijn, J.J.M. Steijger, J.L. Visschers, A. Zondervan, J.R. Calarco, D. DeAngelis, F.W. Hersman, W. Kim, Th.S. Bauer, M.W. Kelder, Z. Papandreou, C. Giusti and F.D. Pacati, Phys. Rev. Lett. 74 (1995) 1712.
- [4] A. Zondervan, L.J. de Bever, E. Jans, J. Konijn, M. Kruijer, J.J.M. Steijger, J.L. Visschers, P.J. Countryman, W.H.A. Hesselink, N. Kalantar-Nayestanaki, L.J.H.M. Kester, J.H. Mitchell, A. Pellegrino, J.R. Calarco, F.W. Hersman, M. Leuschner, T.P. Smith, Th.S. Bauer, M.W. Kelder, C. Giusti, F.D. Pacati, J. Ryckebusch and M. Vanderhaeghen, Nucl. Phys. A 587 (1995) 697.
- [5] C. Giusti and F.D. Pacati, Nucl. Phys. A 535 (1991) 573; Nucl. Phys. A 571 (1994) 694; Nucl. Phys. A 585 (1995) 618.
- [6] C. Giusti, F.D. Pacati and M. Radici, Nucl. Phys. A 546 (1992) 607; S. Boffi, C. Giusti, F.D. Pacati and M. Radici, Nucl. Phys. A 564 (1993) 473.
- [7] C.J.G. Onderwater, K. Allaart, E.C. Aschenauer, Th.S. Bauer, D.J. Boersma, E. Cisbani, S. Frullani, F. Garibaldi, W.J.W. Geurts, D.L. Groep, W.H.A. Hesselink, M. Jodice, E. Jans, N. Kalantar-Nayestanaki, W.-J. Kasdorp, C. Kormanyos, L. Lapikás, J.J. van Leeuwe, R. de Leo, A. Misiejuk, A.R. Pellegrino, R. Perrino, R. Starink, M. Steenbakkers, G. van der Steenhoven, J.J.M. Steijger, M.A. van Uden, G.M. Urciuoli, L.B. Weinstein and H.W. Willering, Phys. Rev. Lett. 78 (1997) 4893.
- [8] C.J.G. Onderwater, Ph.D. thesis, Vrije Universiteit, Amsterdam (1998).
- [9] G. Rosner, Conference on Perspectives in Hadronic Physics, eds. S. Boffi, C. Ciofi degli Atti, and M.M. Giannini (World Scientific, Singapore), in press.
- [10] P. Bartsch, D. Baumann, R. Böhm, T. Caprano, S. Derber, M. Ding, A. Ebbes, I. Ewald, J. Friedrich, J.M. Friedrich, R. Geiges, P. Jennewein, M. Kahrau, M. Korn, K.W. Krygier, A. Liesenfeld, H. Merkel, K. Merle, P. Merle, U. Müller, R. Neuhausen, Th. Pospischil, G. Rosner (spokesperson), H. Schmieden, A. Wagner, Th. Walcher, M. Weis, S. Wolf, MAMI proposal Nr: A1/1-97.
- [11] C. Giusti and F.D. Pacati, Nucl. Phys. A 615 (1997) 373.
- [12] C. Giusti, F.D. Pacati, K. Allaart, W.J.W. Geurts, W.H. Dickhoff and H. Müther, Phys. Rev. C 57 (1998) 1691.
- [13] W.J.W. Geurts, K. Allaart, W.H. Dickhoff and H. Müther, Phys. Rev. C 54 (1996) 1144.
- [14] J. Ryckebusch, L. Machenil, M. Vanderhaengen, and M. Waroquier, Phys. Lett. B 291 (1992) 213; L. Machenil, M. Vanderhaengen, J. Ryckebusch, and M. Waroquier, Phys. Lett. B 316 (1993) 17;

J. Ryckebusch, L. Machenil, M. Vanderhaengen, V. Van der Sluys and M. Waroquier, Phys. Rev. C 49 (1994) 2704;

J. Ryckebusch, L. Machenil, M. Vanderhaengen, and M. Waroquier, Nucl. Phys. A 568 (1994) 828;

M. Vanderhaengen, L. Machenil, J. Ryckebusch, and M. Waroquier, Nucl. Phys. A 580 (1994) 551.

[15] J. Ryckebusch, D. Debruyne and W. Van Nespen, Phys. Rev. C 57 (1998) 1319.

[16] J. Arends, J. Eyimk, H. Hartmann, A. Hegerath, B. Mecking, G. Nöldeke, and H. Rost, Z. Phys. (1980) 103.

[17] M. Kanazawa, S. Homma, M. Koike, Y. Murata, H. Okuno, F. Soga, N. Yoshikawa and A. Sasaki, Phys. Rev. C 35 (1987) 1828.

[18] J.C. McGeorge, I.J.D. MacGregor, S.N. Dancer, J.R.M. Annand, I. Anthony, G.I. Crawford, S.J. Hall, P.D. Harty, J.D., Kellie, G.J. Miller, R.O. Owens, P.A. Wallace, D. Branford, A.C. Shotter, B. Schoch, R. Beck, H. Schmieden and J.M. Vogt, Phys. Rev. C 51 (1995) 1967.

[19] P. Grabmayr, J. Ahrens, J.R.M. Annand, I. Anthony, D. Branford, G.E. Cross, T. Davinson, S.J. Hall, P.D. Harty, T. Hehl, J.D. Kellie, Th. Lamparter, I.J.D. MacGregor, J.A. MacKenzie, J.C. McGeorge, G.J. Miller, R.O. Owens, M. Sauer, R. Schneider, K. Spaeth and G.J. Wagner, Phys. Lett. B 370 (1996) 17;
 P.D. Harty, I.J.D. MacGregor, P. Grabmayr, J. Ahrens, J.R.M. Annand, I. Anthony, R. Beck, D. Branford, G.E. Cross, T. Davinson, S.J. Hall, T. Hehl, J.D. Kellie, Th. Lamparter, J.A. MacKenzie, J.C. McGeorge, G.J. Miller, R.O. Owens, M. Sauer, R. Schneider and K. Spaeth, Phys. Lett. B 380 (1996) 247;
 Th. Lamparter, J. Ahrens, J.R.M. Annand, I. Anthony, R. Beck, D. Branford, G.E. Cross, T. Davinson, P. Grabmayr, S.J. Hall, P.D. Harty, T. Hehl, J.D. Kellie, I.J.D. MacGregor, J.A. MacKenzie, J.C. McGeorge, G.J. Miller, R.O. Owens, M. Sauer, R. Schneider, K. Spaeth and G.J. Wagner, Z. Phys. A 355 (1996) 1.

[20] I.J.D. MacGregor, T. T-H. Yau, J. Ahrens, J.R.M. Annand, R. Beck, D. Branford, P. Grabmayr, S.J. Hall, P.D. Harty, T. Hehl, J.D. Kellie, Th. Lamparter, M. Liang, J.A. MacKenzie, S. McAllister, J.C. McGeorge, R.O. Owens, J. Ryckebusch, M. Sauer, R. Schneider and D.P. Watts, Phys. Rev. Lett. 80 (1998) 245.

[21] L. Isaksson, J-O. Adler, B-E. Andersson, K.I. Blomqvist, A. Sandell, B. Schröder, P. Grabmayr, S. Klein, G. Mauser, A. Mondry, J.R.M. Annand, G.I. Crawford, J.C. McGeorge and G.J. Miller, Proc. Second Workshop on Electromagnetically Induced Two-Nucleon Emission, ed. by J. Ryckebusch and M. Waroquier, Gent (1995) p. 301; L. Isaksson, Ph.D. thesis, University of Lund, (1996).

[22] R.C. Carrasco and E. Oset, Nucl. Phys. A 536 (1992) 445;
 R.C. Carrasco, E. Oset and L.L. Salcedo, Nucl. Phys. A 54 (1992) 585;
 R.C. Carrasco, M.J. Vicente Vacas and E. Oset, Nucl. Phys. A 570 (1994) 701.

[23] J. Ahrens, J.R.M. Annand, R. Beck, D. Branford, P. Grabmayr (spokesperson), S.J. Hall, T. Hehl, D.J. Ireland, J.D. Kellie, I.J.D. MacGregor, M. Mayer, J.C. McGeorge, F.A. Natter, R.O. Owens, M. Sauer, G.J. Wagner and S. Wunderlich, MAMI proposal Nr: A2/4-97.

[24] P. Wilhelm, H. Arenhövel, C. Giusti, and F. D. Pacati, Z. Phys. A 359 (1997) 467.

- [25] R. Lindgren, V. Gladyshev, H. Baghaei, A. Caracappa, A. Cichocki, R. Finlay, T. Gresko, K. Hicks, S. Hoblit, M. Khandakar, O. Kistner, M. Lucas, L. Miceli, B. Norum, J. Rappaport, A. Sandorfi, R. Sealock, L. Smith, C. Thorn, S. Thornton, C. Whisnant, C. Giusti, F.D. Pacati and J. Ryckebusch, to be published
- [26] H. Müther and P.U. Sauer, Computational Nuclear Physics, eds. K.-H. Langanke, J.A. Maruhn and S.E. Koonin, (Springer, New York, 1993).
- [27] R.D. Peccei, Phys. Rev. 176 (1968) 1812; 181 (1969) 1902.
- [28] Th. Wilbois, P. Wilhelm and H. Arenhövel, Phys. Rev. C 54 (1996) 3311.
- [29] B.H. Bransden and R.G. Moorhouse, The Pion-Nucleon System, (Princeton, University Press, Princeton, 1973).
- [30] P. Wilhelm, J.A. Niskanen and H. Arenhövel, Nucl. Phys. A 597 (1996) 613.
- [31] F. Ajzenberg-Selove, Nucl. Phys. A 523 (1991) 1.
- [32] A. Nadasen, P. Schwandt, P.P. Singh, W.W. Jacobs, A.D. Bacher, P.T. Debevec, M.D. Kaitchuk and J.T. Meek, Phys. Rev. C 23 (1981) 1023.
- [33] L.R.B. Elton and A. Swift, Nucl. Phys. A 94 (1967) 52.
- [34] C.C. Gearhart, Ph.D. thesis, Washington University, St. Louis (1994); C.C. Gearhart and W.H. Dickhoff, private communication.
- [35] J.W. Clark, in The Many-body problem: Jastrow correlations versus Brueckner theory, ed. by R. Guardiola and J. Ros, Lecture Notes in Physics, vol. 138 (Springer, Berlin 1981) p. 184.
- [36] T. Ohmura, N. Morita and M. Yamada, Prog. Theor. Phys. 15 (1956) 222.

TABLES

$J^\pi T$	hole		n	N	
$1_1^+ 0$	$(p_{1/2})^{-2}$	$^3S_1; L = 0$	1	0	0.14
		$^3S_1; L = 0$	0	1	-0.14
		$^3S_1; L = 2$	0	0	0.61
		$^1P_1; L = 1$	0	0	-0.47
		$^3D_1; L = 0$	0	0	-0.61
$0^+ 1$	$(p_{1/2})^{-2}$	$^1S_0; L = 0$	1	0	-0.41
		$^1S_0; L = 0$	0	1	0.41
		$^3P_1; L = 1$	0	0	0.82
$1_2^+ 0$	$(p_{1/2}p_{3/2})^{-1}$	$^3S_1; L = 0$	1	0	-0.54
		$^3S_1; L = 0$	0	1	0.54
		$^3S_1; L = 2$	0	0	0.30
		$^1P_1; L = 1$	0	0	0.47
		$^3D_1; L = 0$	0	0	-0.30
$2^+ 0$	$(p_{1/2}p_{3/2})^{-1}$	$^3S_1; L = 2$	0	0	-0.71
		$^3D_2; L = 0$	0	0	-0.71
$3^+ 0$	$(p_{3/2})^{-2}$	$^3S_1; L = 2$	0	0	0.71
		$^3D_3; L = 0$	0	0	-0.71

TABLE I. Proton-neutron removal amplitudes from ^{16}O for states of ^{14}N in a h.o. approximation and for different relative $^{2S+1}l_j$ states. L is the CM angular momentum.

$J^\pi T$	hole		n	N	c^i
$0^+ 1$	$(p_{1/2})^{-2}$	$^1S_0; L = 0$	1	0	-0.41
		$^1S_0; L = 0$	0	1	0.41
		$^3P_1; L = 1$	0	0	0.51
$2^+ 1$	$(p_{1/2}p_{3/2})^{-1}$	$^1S_0; L = 2$	0	0	-0.58
		$^3P_1; L = 1$	0	0	0.29
		$^3P_2; L = 1$	0	0	0.50
		$^1D_2; L = 2$	0	0	0.49
$1^+ 1$	$(p_{1/2}p_{3/2})^{-1}$	$^3P_0; L = 1$	0	0	0.58
		$^3P_1; L = 1$	0	0	0.50
		$^3P_2; L = 1$	0	0	-0.65

TABLE II. Two-proton removal amplitudes from ^{16}O for states of ^{14}C in a h.o. approximation and for different relative $^{2S+1}l_j$ states. L is the CM angular momentum. The amplitudes are compared with the corresponding coefficients c^i in Eq. (5), obtained from the calculation of the spectral function of ref. [13].

FIGURES

FIG. 1. The differential cross section of the reaction $^{16}\text{O}(\gamma, \text{pn})^{14}\text{N}$, as a function of the angle γ_1 , in coplanar symmetrical kinematics at $E_\gamma = 100$ MeV, for the transitions to the low-lying states in ^{14}N : 1_1^+ ($E_{2\text{m}} = 22.96$ MeV), 0^+ ($E_{2\text{m}} = 25.27$ MeV), 1_2^+ ($E_{2\text{m}} = 26.91$ MeV), 2^+ ($E_{2\text{m}} = 29.99$ MeV), 3^+ ($E_{2\text{m}} = 34.01$ MeV). The optical potential is taken from ref. [32], the single-particle wave functions from ref. [33] and the correlation function from ref. [34]. Separate contributions of the one-body current (1-B) and of its sum with the two-body seagull (SEA) and pion-in-flight (π) currents are drawn. The solid lines give the total cross section, where also the Δ current (Δ) is added.

FIG. 2. The differential cross section of the reaction $^{16}\text{O}(\gamma, \text{pn})^{14}\text{N}$, as a function of the angle γ_1 , in the same kinematics and for the same transitions as in Fig. 1. Optical potential, single-particle wave functions and correlation function as in Fig. 1. The solid lines are the same as in Fig. 1. Separate contributions of the Δ , seagull, pion-in-flight currents and of the sum of seagull and pion-in-flight currents are drawn.

FIG. 3. The differential cross section of the reaction $^{16}\text{O}(\gamma, \text{pn})^{14}\text{N}$, as a function of the angle γ_1 , in coplanar symmetrical kinematics at $E_\gamma = 300$ MeV, for the same transitions, under the same conditions and with same line convention as in Fig. 1.

FIG. 4. The differential cross section of the reaction $^{16}\text{O}(\gamma, \text{pn})^{14}\text{N}$, as a function of the angle γ_1 , in coplanar symmetrical kinematics at $E_\gamma = 300$ MeV, for the same transitions, under the same conditions and with same line convention as in Fig. 2.

FIG. 5. The differential cross section of the reaction $^{16}\text{O}(\gamma, \text{pn})^{14}\text{N}$, as a function of the photon energy, for a fixed value of the angle γ_1 , in coplanar symmetrical kinematics, for the same transitions as in Fig. 1. Optical potential, single-particle wave functions and correlation function as in Fig. 1. Line convention as in Fig. 1.

FIG. 6. The differential cross section of the reaction $^{16}\text{O}(\gamma, \text{pn})^{14}\text{N}$, as a function of the photon energy, for a fixed value of the angle γ_1 , in coplanar symmetrical kinematics, for the same transitions, under the same conditions and with same line convention as in Fig. 2.

FIG. 7. The photon asymmetry of the reaction $^{16}\text{O}(\vec{\gamma}, \text{pn})^{14}\text{N}$, as a function of the angle γ_1 , in the coplanar symmetrical kinematics at $E_\gamma = 100$ MeV, for the same transitions, under the same conditions and with same line convention as in Fig. 1.

FIG. 8. The photon asymmetry of the reaction $^{16}\text{O}(\vec{\gamma}, \text{pn})^{14}\text{N}$, as a function of the angle γ_1 , in the coplanar symmetrical kinematics at $E_\gamma = 100$ MeV, for the same transitions, under the same conditions and with same line convention as in Fig. 2.

FIG. 9. The photon asymmetry of the reaction $^{16}\text{O}(\vec{\gamma}, \text{pn})^{14}\text{N}$, as a function of the angle γ_1 , in the coplanar symmetrical kinematics at $E_\gamma = 300$ MeV, for the same transitions, under the same conditions and with same line convention as in Fig. 3.

FIG. 10. The photon asymmetry of the reaction $^{16}\text{O}(\vec{\gamma}, \text{pn})^{14}\text{N}$, as a function of the angle γ_1 , in the coplanar symmetrical kinematics at $E_\gamma = 300$ MeV, for the same transitions, under the same conditions and with same line convention as in Fig. 4.

FIG. 11. The differential cross section of the reaction $^{16}\text{O}(\gamma, \text{pp})^{14}\text{C}$, as a function of the angle γ_1 , in coplanar symmetrical kinematics at $E_\gamma = 100$ MeV, for the transitions to the low-lying states in ^{14}C : 0_1^+ ($E_{2m} = 22.33$ MeV), 2^+ ($E_{2m} = 30.00$ MeV), 1^+ ($E_{2m} = 33.64$ MeV). The defect functions for the Bonn-A potential and the optical potential of ref. [32] are used. Separate contributions of the one-body and two-body Δ currents are drawn. The solid lines give the total cross sections, produced by the sum of the one-body and Δ currents.

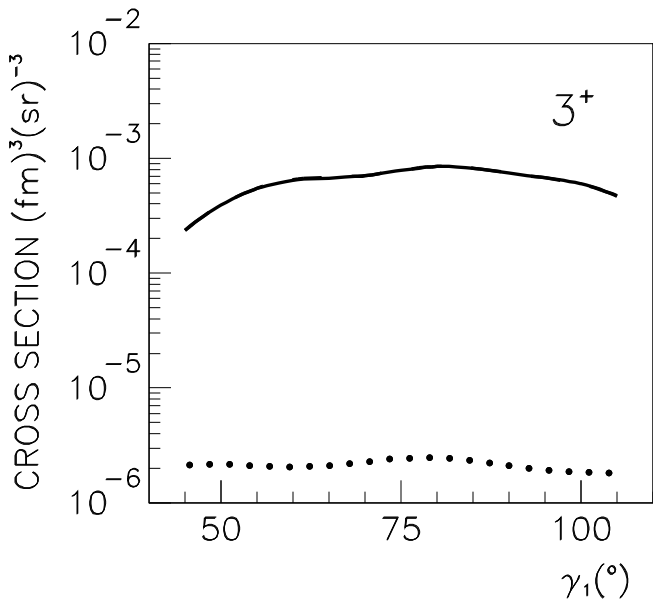
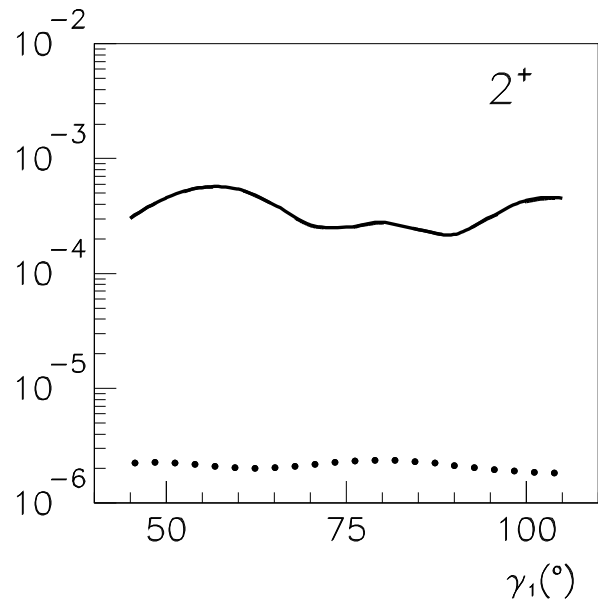
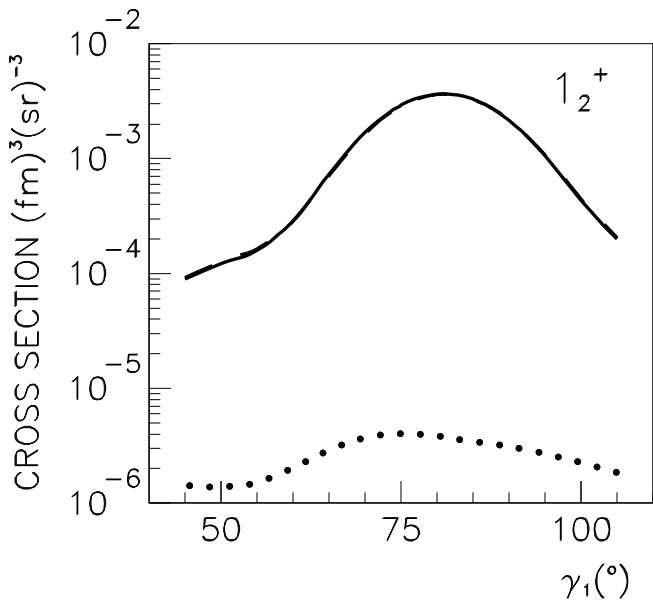
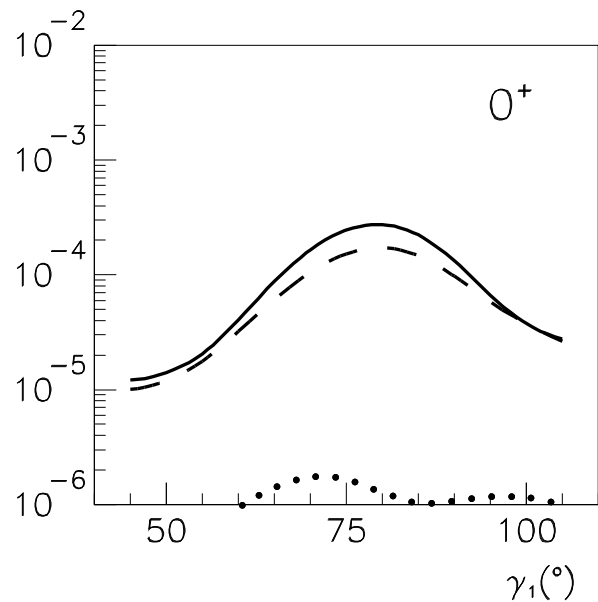
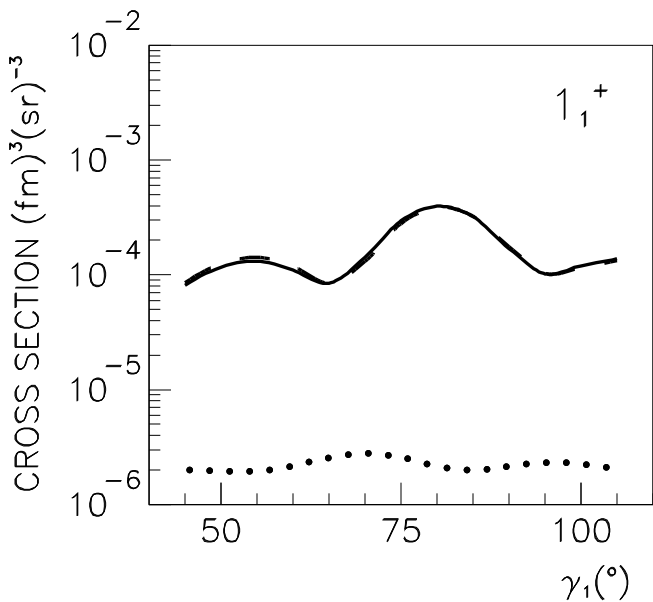
FIG. 12. The differential cross section of the reaction $^{16}\text{O}(\gamma, \text{pp})^{14}\text{C}$, as a function of the angle γ_1 , in the same kinematics and for the same transitions as in Fig. 11. Defect functions and optical potential as in Fig. 11. The solid lines are the same as in Fig. 11. Separate contributions of different partial waves of relative motion are drawn.

FIG. 13. The differential cross section of the reaction $^{16}\text{O}(\gamma, \text{pp})^{14}\text{C}$, as a function of the angle γ_1 , in coplanar symmetrical kinematics at $E_\gamma = 300$ MeV, for the same transitions, under the same conditions and with same line convention as in Fig. 12.

FIG. 14. The differential cross section of the reaction $^{16}\text{O}(\gamma, \text{pp})^{14}\text{C}$, as a function of the angle γ_1 , in coplanar symmetrical kinematics at $E_\gamma = 100$ MeV, for the transitions to the 0^+ and 2^+ states in ^{14}C . The solid and dashed lines are calculated with the defect functions of the Bonn-A and Reid potentials, respectively; the dotted and dot-dashed lines give the corresponding separate contributions of the one-body current. The optical potential is taken from ref. [32]

FIG. 15. The photon asymmetry of the reaction $^{16}\text{O}(\vec{\gamma}, \text{pp})^{14}\text{C}$, as a function of the angle γ_1 , for the transitions the 2^+ and 1^+ states in ^{14}C in the same kinematics as in Fig. 12. Defect functions, optical potential and line convention as in Fig. 12.

FIG. 16. The photon asymmetry of the reaction $^{16}\text{O}(\vec{\gamma}, \text{pp})^{14}\text{C}$, as a function of the angle γ_1 , in coplanar symmetrical kinematics at $E_\gamma = 100$ MeV, for the transition to the 2^+ state in ^{14}C . Optical potential and line convention as in Fig. 14.



1-B + SEA + π + Δ
 1-B + SEA + π
 1-B

Fig.1

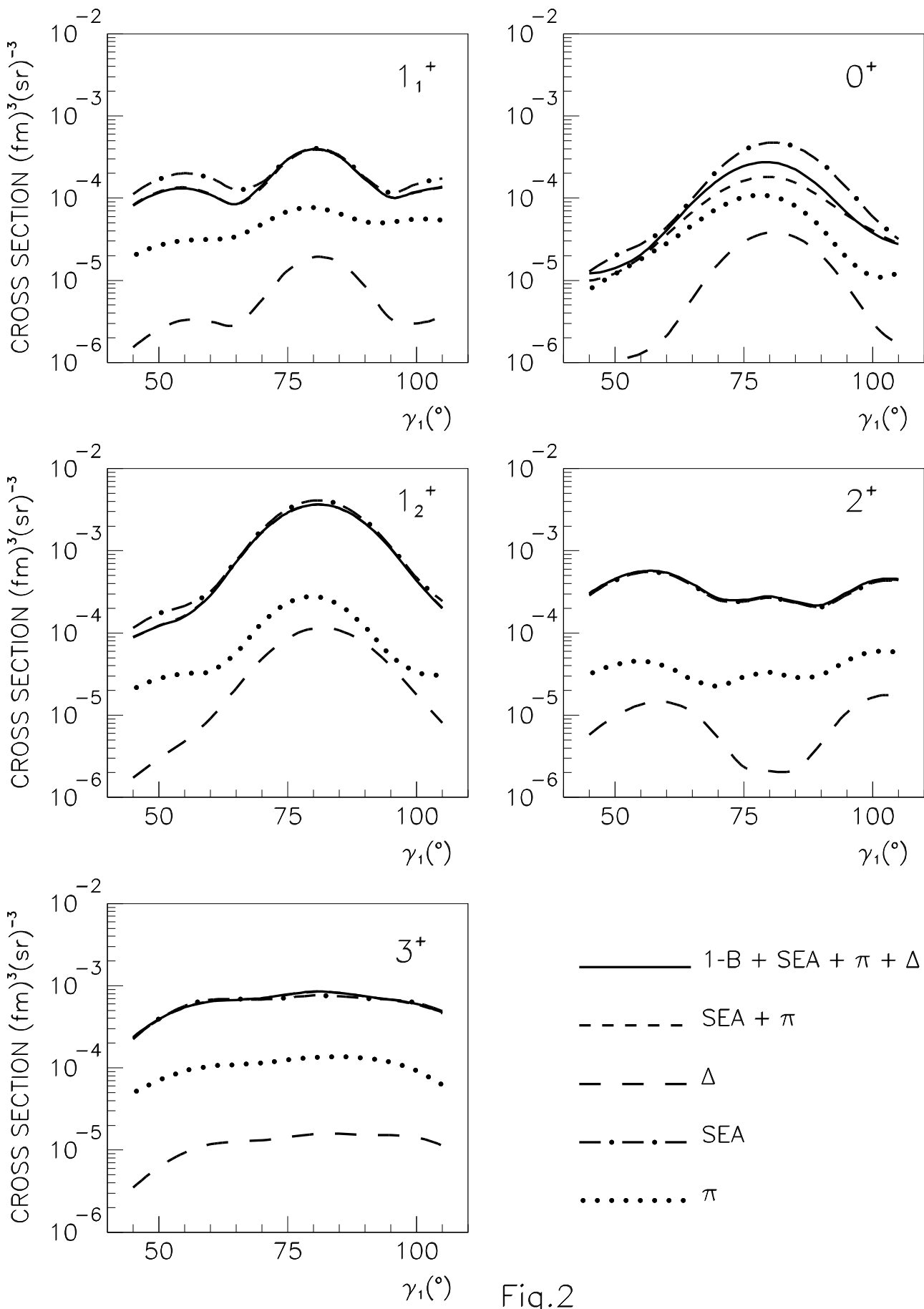


Fig.2

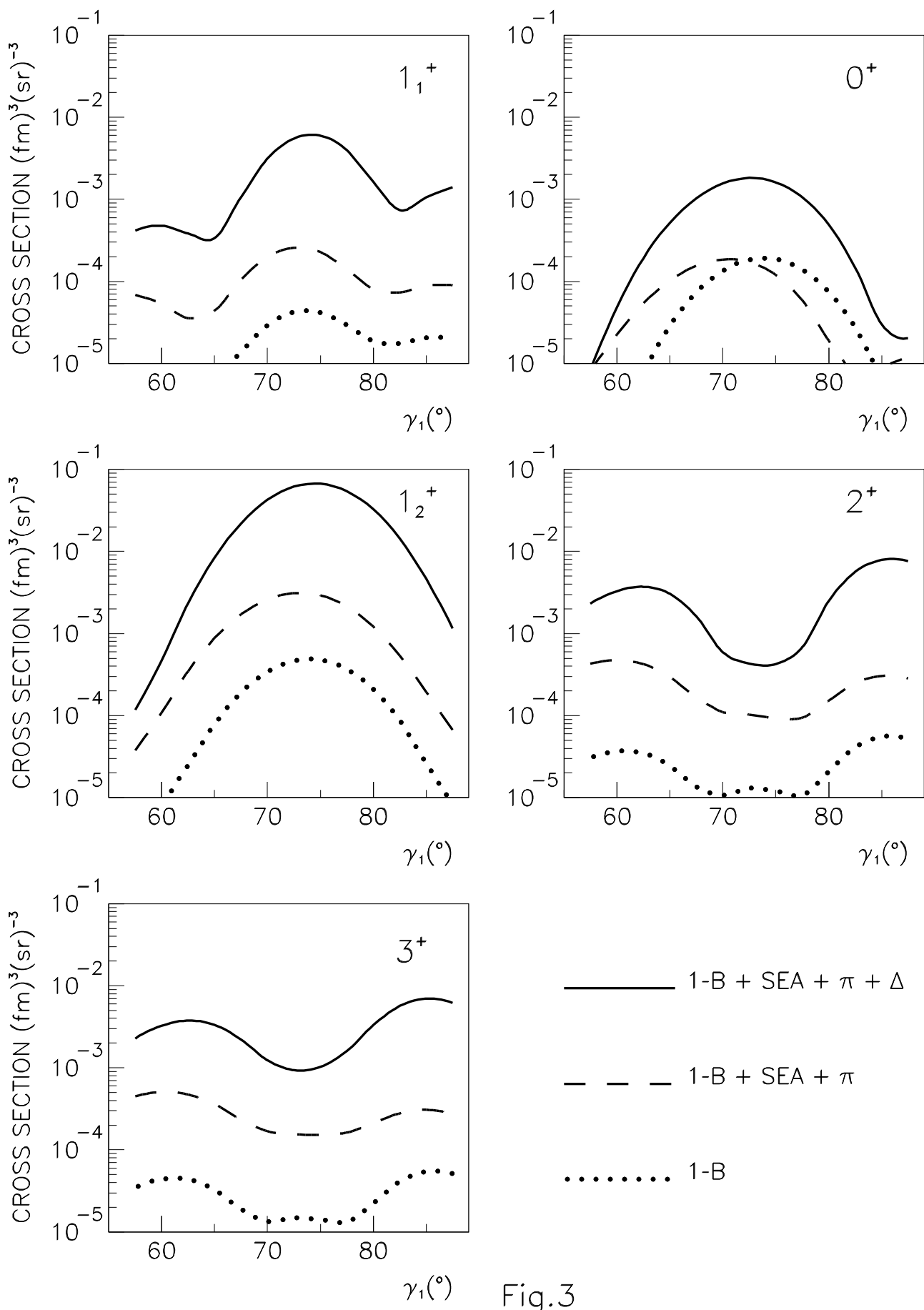


Fig.3

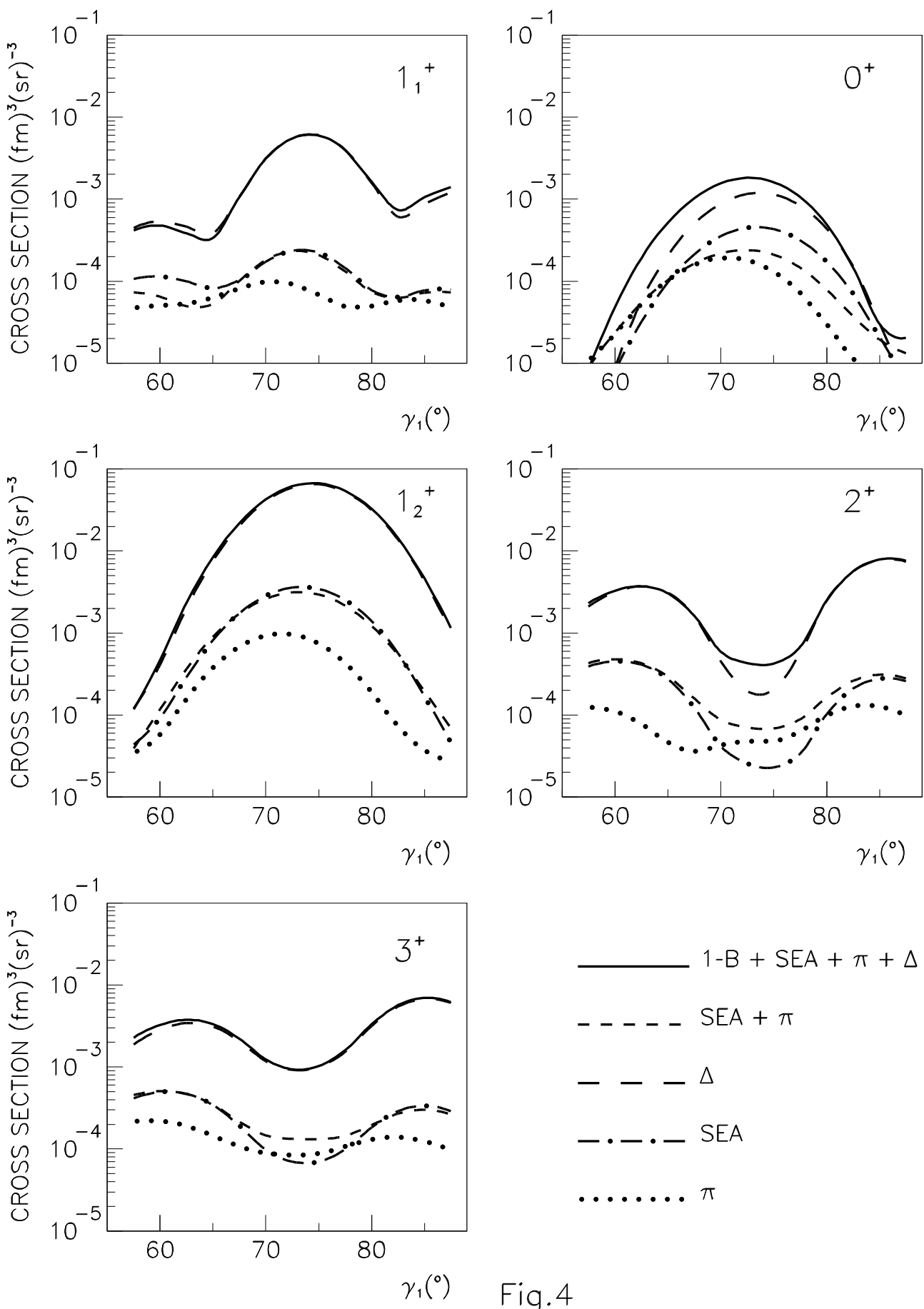


Fig.4

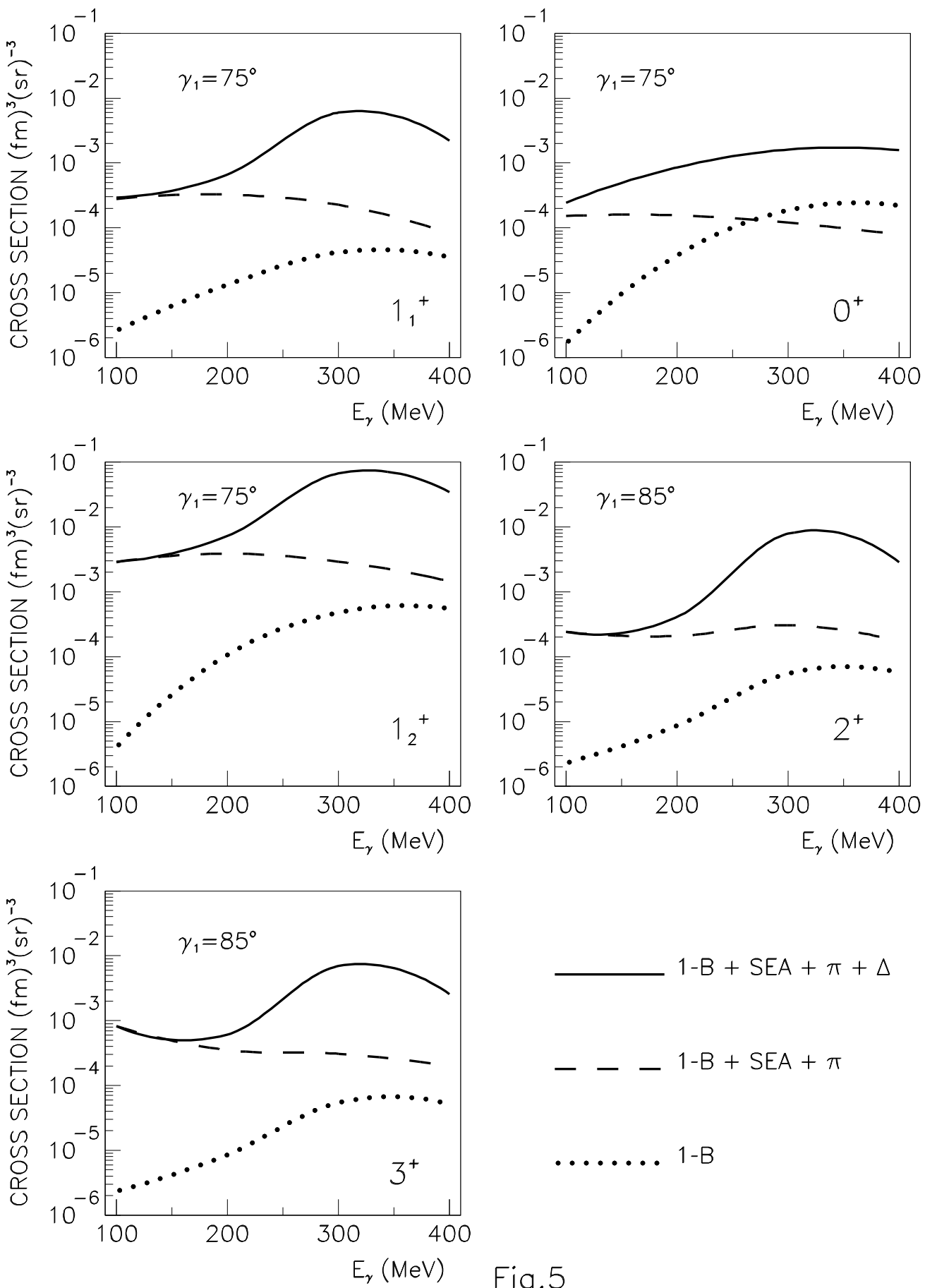


Fig.5

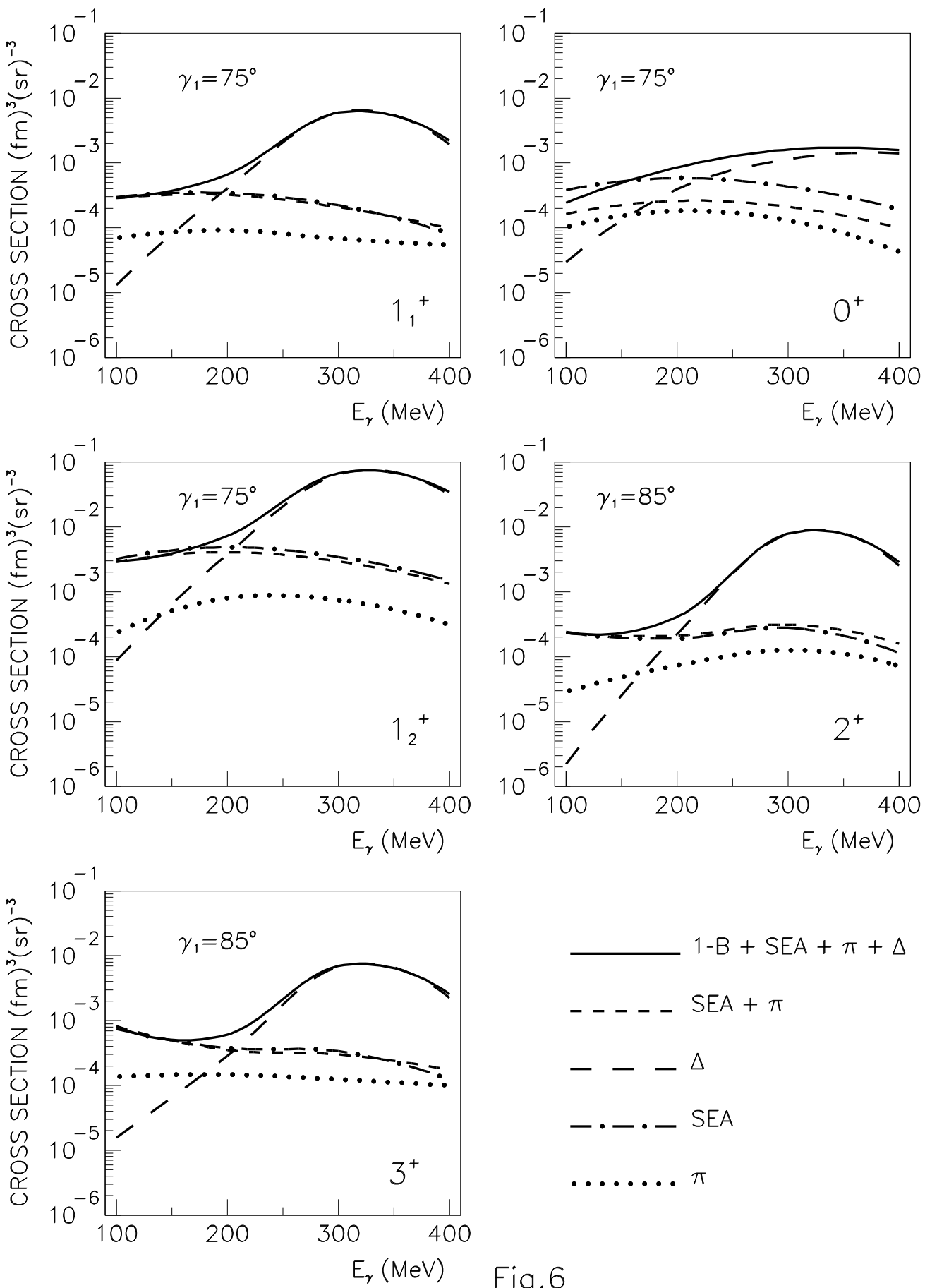


Fig.6

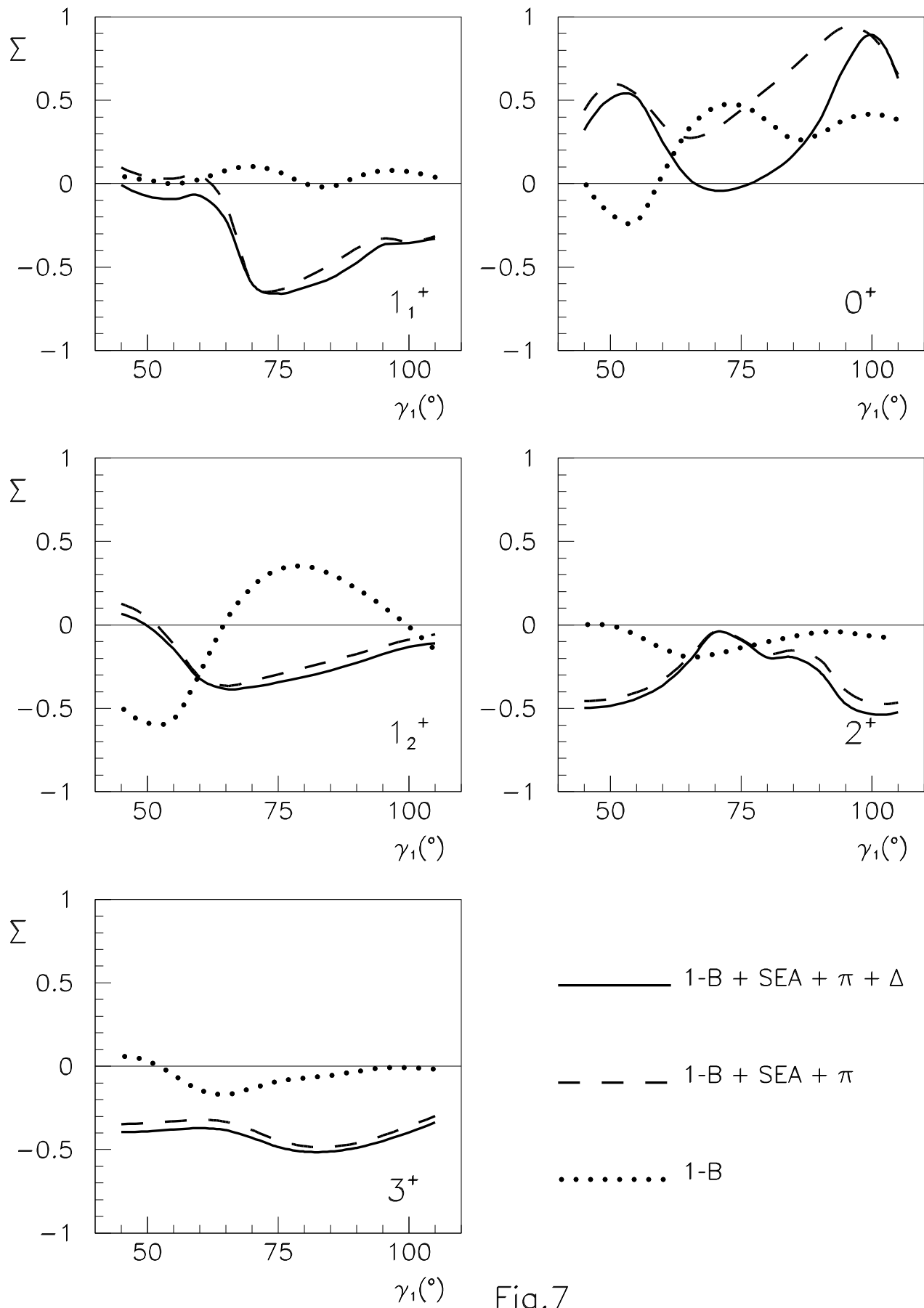


Fig.7

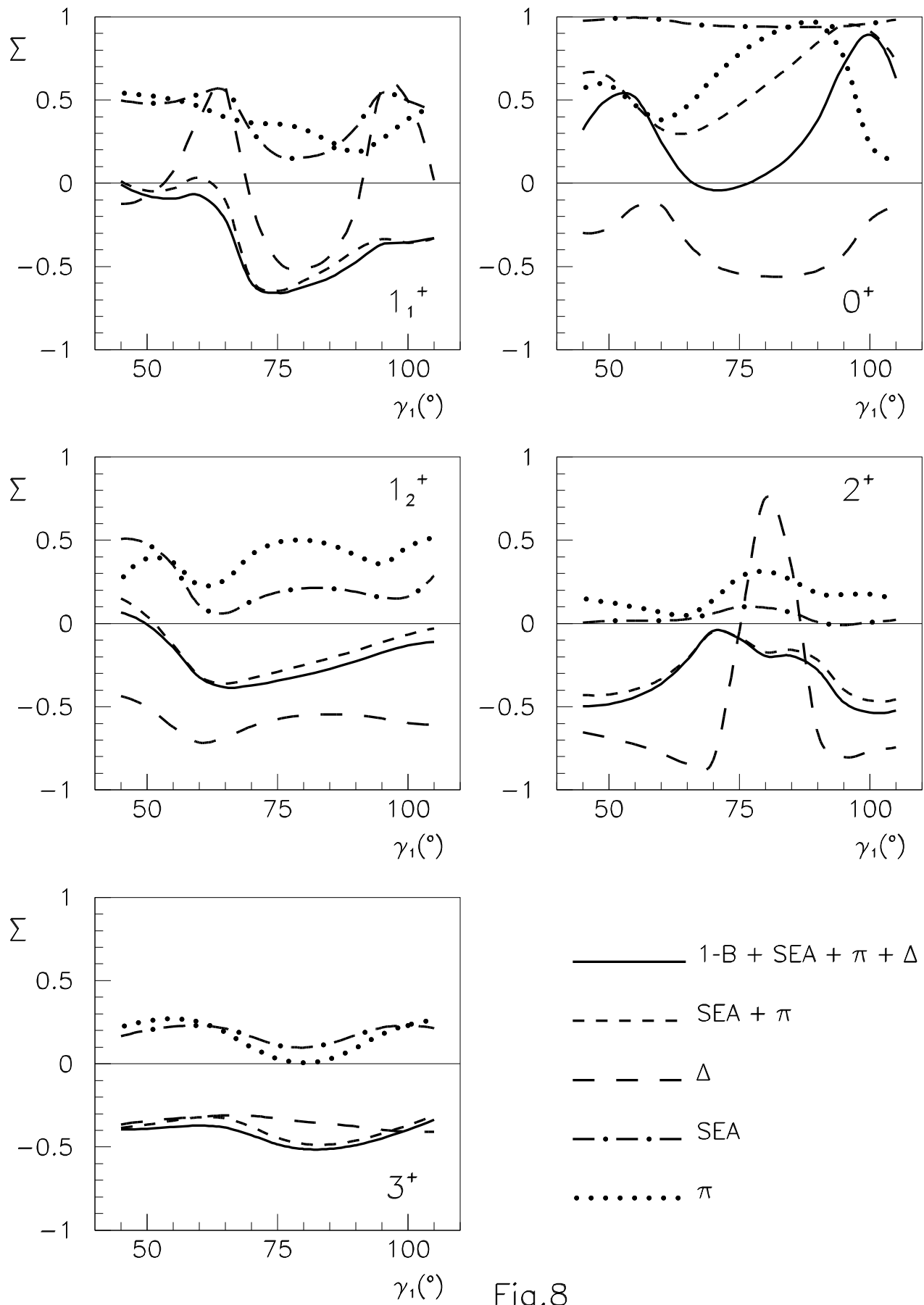


Fig.8

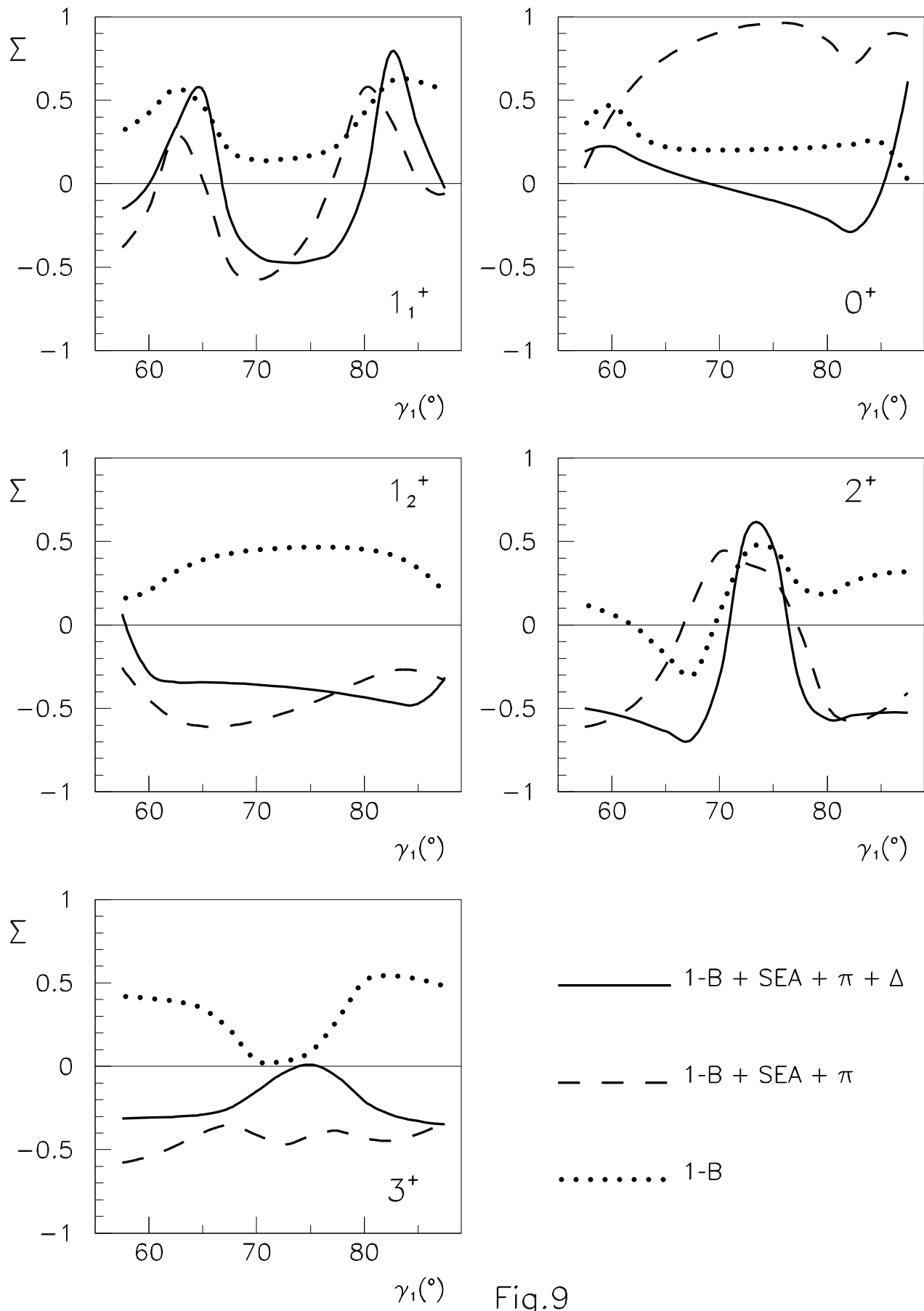


Fig.9

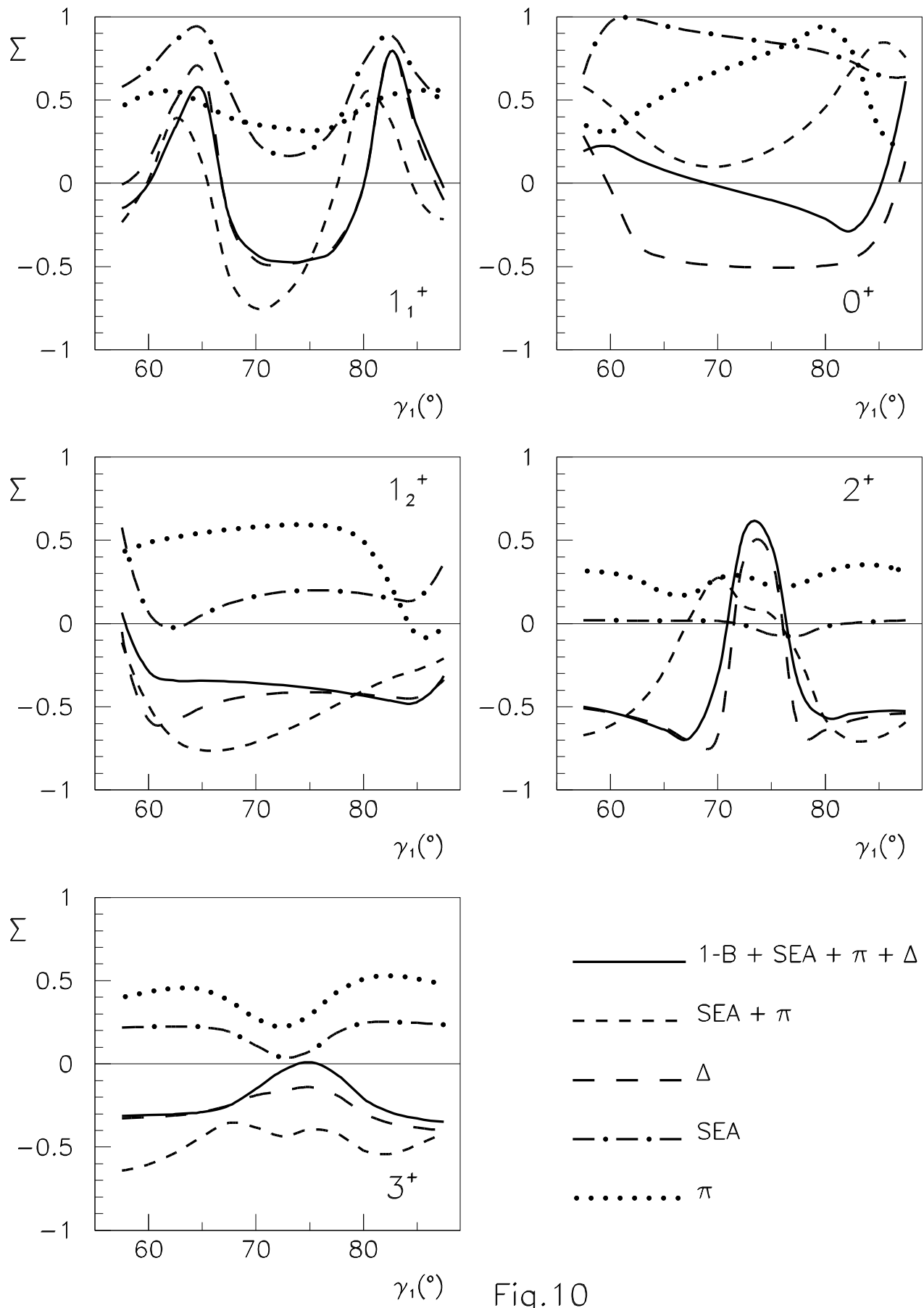
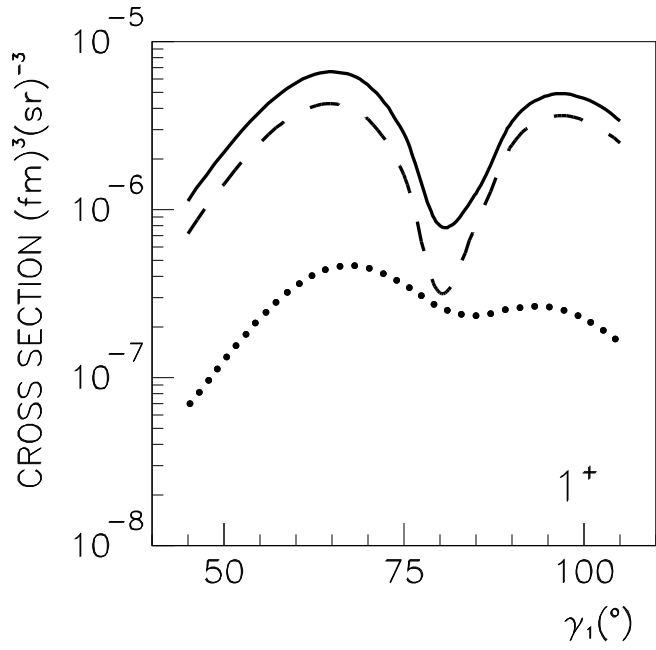
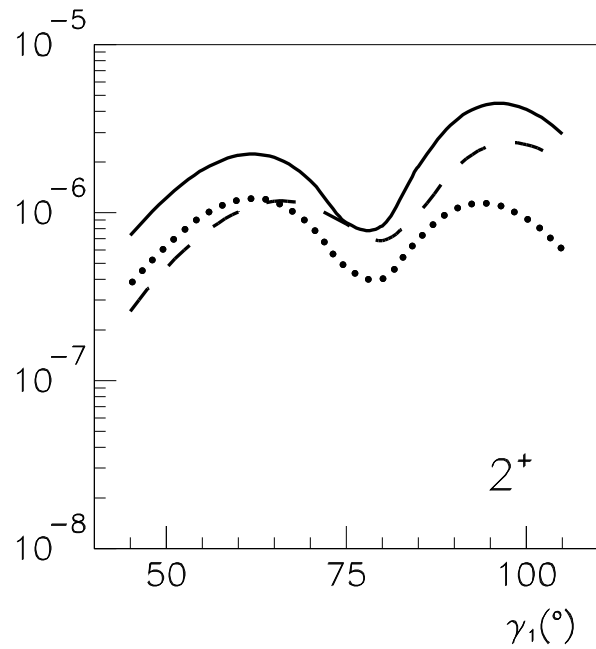
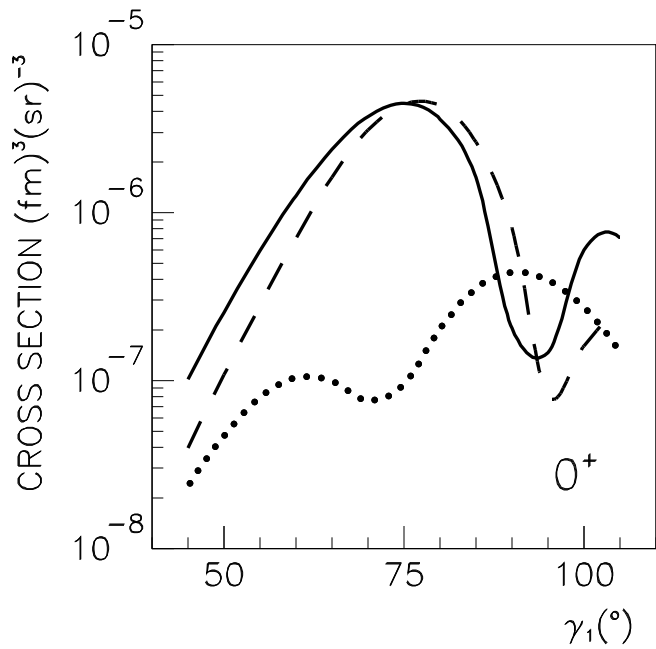


Fig.10

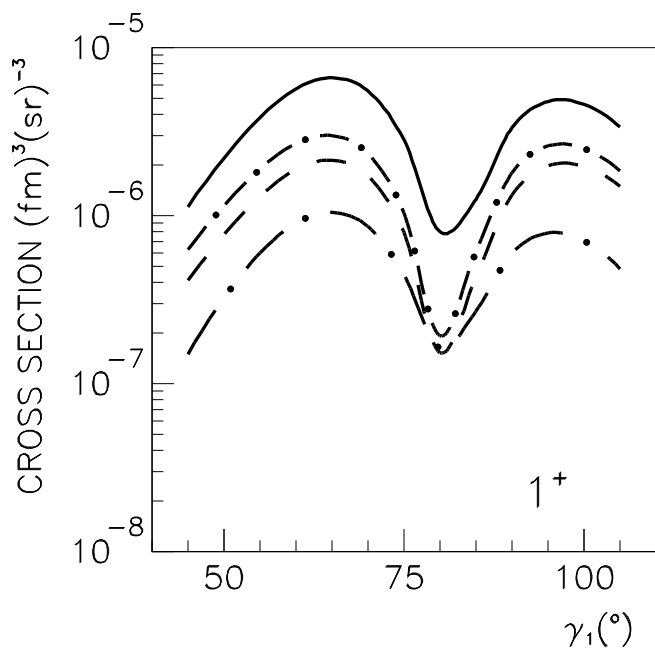
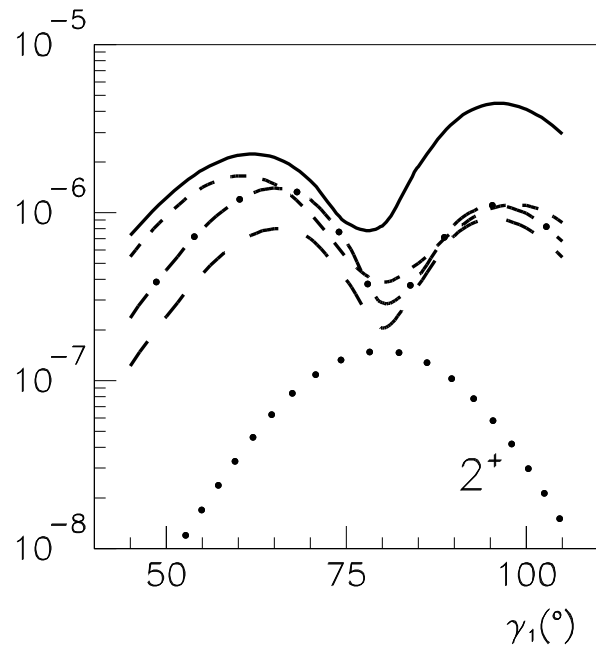
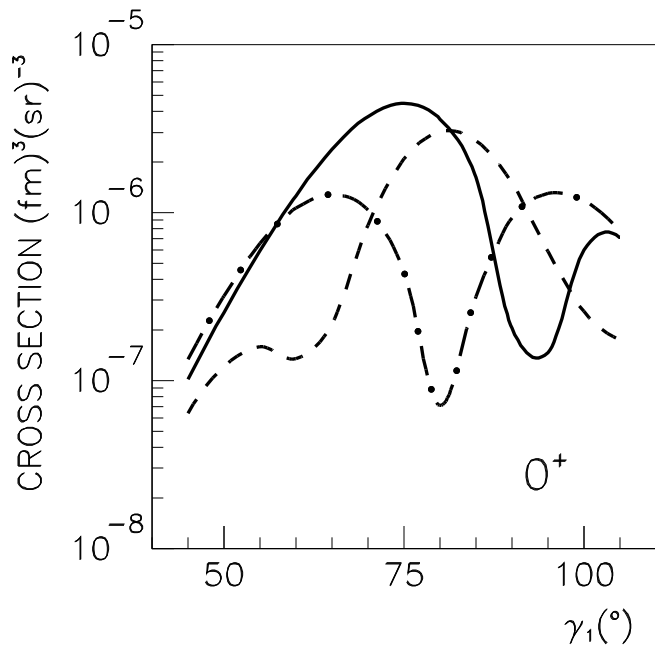


— 1-B + Δ

- - - Δ

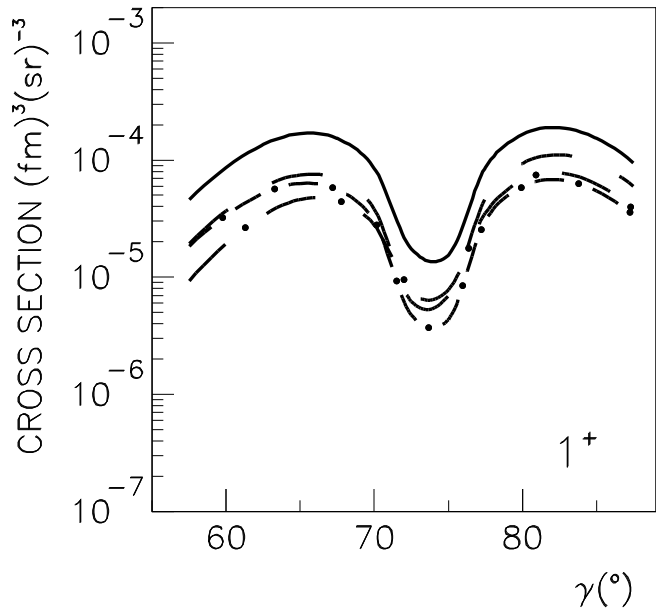
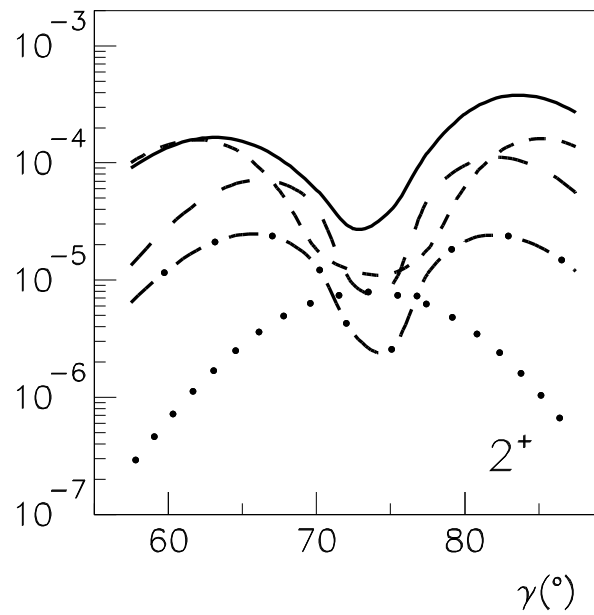
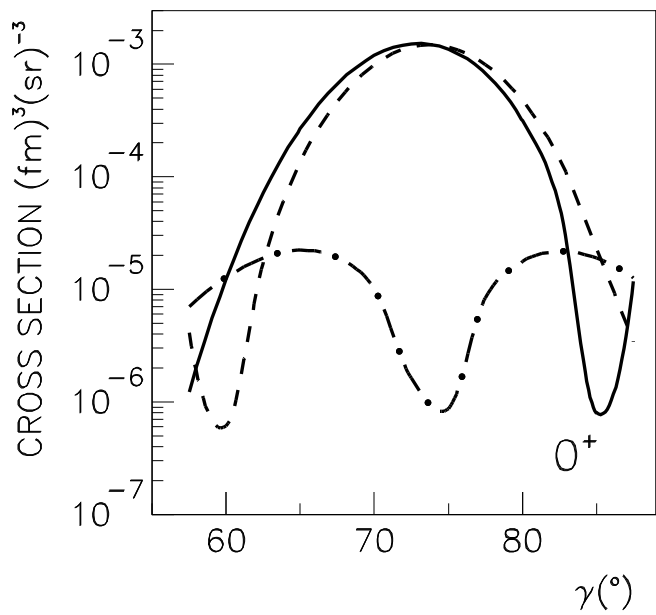
..... 1-B

Fig.11



$1S_0$	$\cdots \cdots \cdots$
$3P_2$	$- - - - -$
$3P_1$	$- - - - -$
$3P_0$	$- - - - -$
$1D_2$	$\cdot \cdot \cdot \cdot \cdot \cdot \cdot \cdot \cdot$

Fig.12



$1S_0$	$\cdots \cdots \cdots$
$3P_2$	$- - - - -$
$3P_1$	$- - - \cdot - - -$
$3P_0$	$- \cdot - \cdot -$
$1D_2$	$\cdot \cdot \cdot \cdot \cdot \cdot \cdot \cdot$

Fig.13

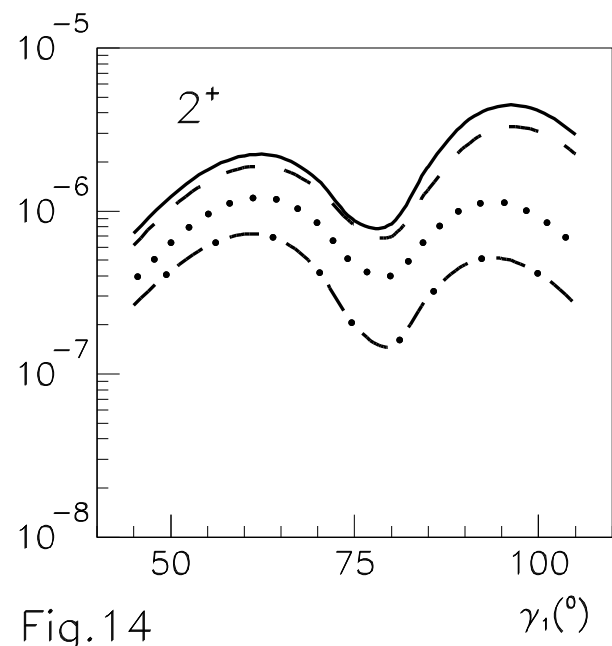
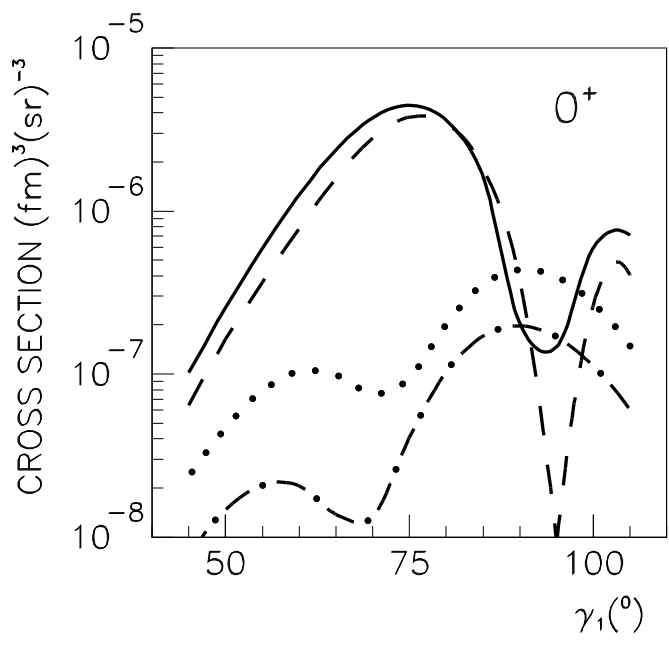


Fig.14

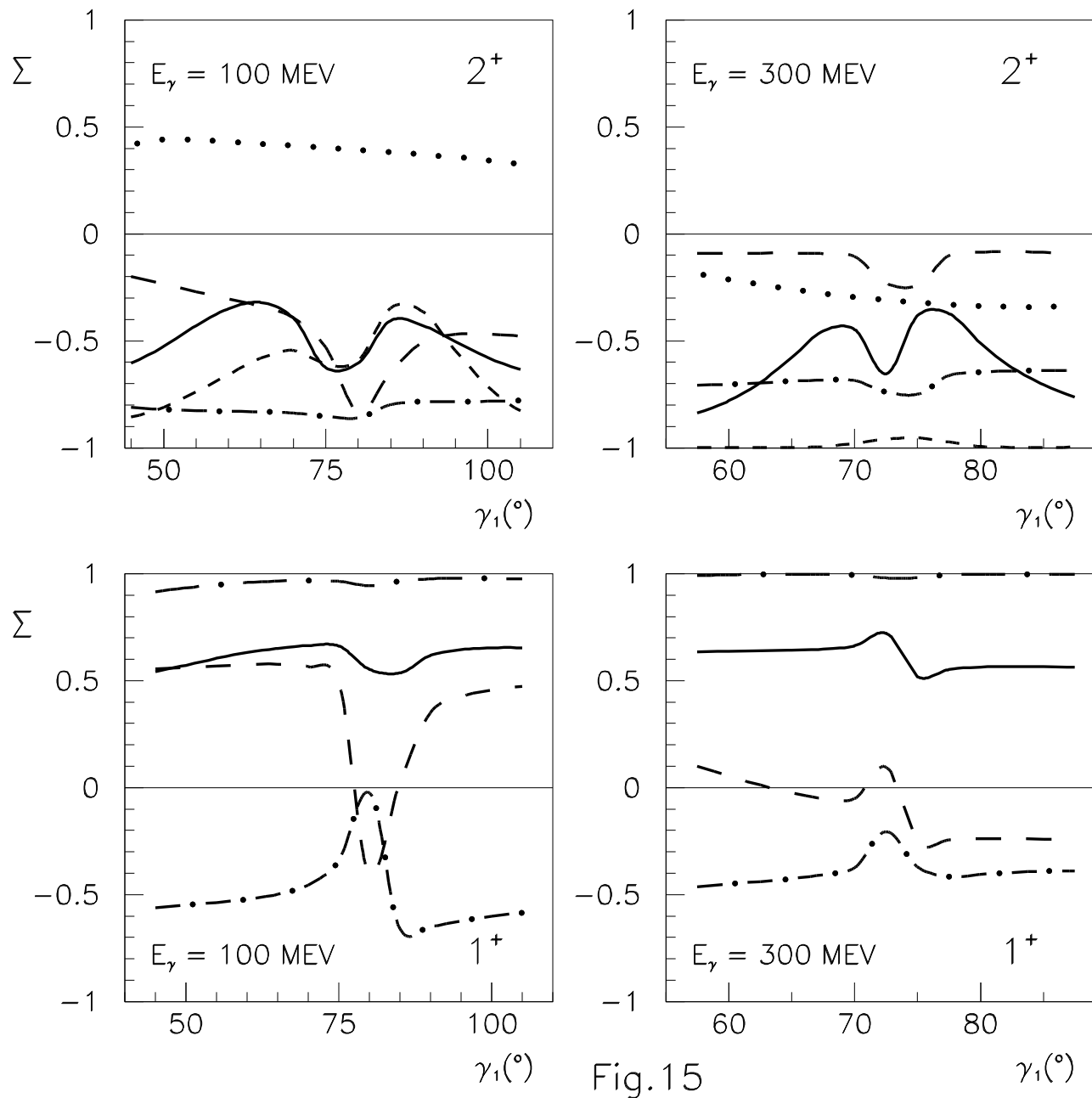


Fig.15

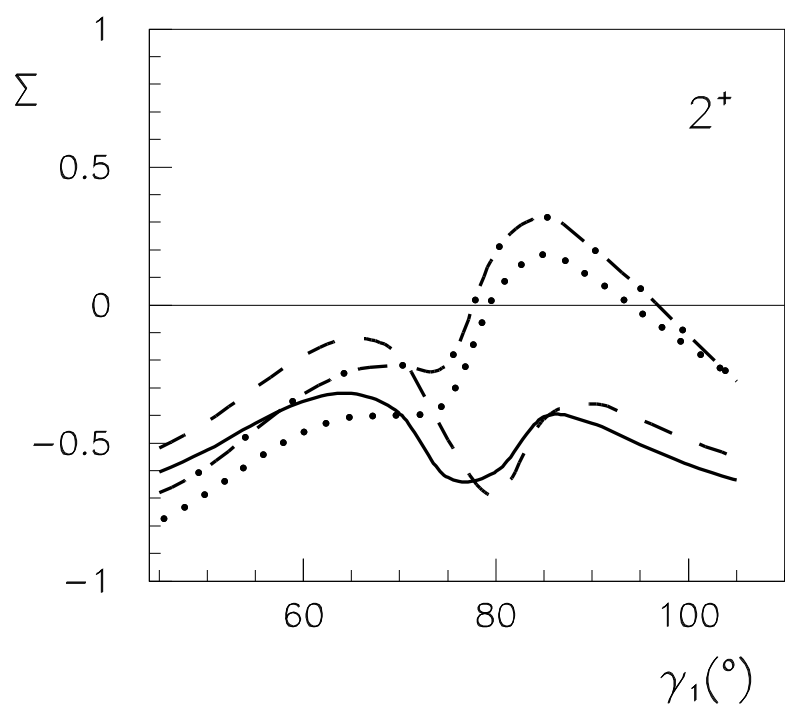


Fig.16